

Two interface type numerical methods for computing hyperbolic systems with geometrical source terms having concentrations*

Shi Jin [†] and Xin Wen [‡]

Abstract

We propose two simple well-balanced methods for hyperbolic system with geometrical source terms having concentrations. Physical problems under consideration include the shallow water equations with topography, and the quasi one-dimensional isothermal nozzle flows. These two methods use the numerical fluxes already obtained from the corresponding homogeneous systems in the source terms, and one only needs a black-box (approximate) Riemann solver for the homogeneous system. Compared to our previous method developed in [17], these methods avoid the Newton iterations in the evaluation of the source term. Numerical experiments demonstrate that both methods give good numerical approximations to the sub- and super-critical flows. With a transonic fix, both methods also capture with a high resolution the transonic flows over the concentration. These methods are applicable to both unsteady and steady state computations.

*Research supported in part by NSF grant No. DMS-0305080, NSFC under the Project 10228101 and the Basic Research Projects of Tsinghua University under the Project JC2002010.

[†]Department of Mathematics, University of Wisconsin, Madison, WI 53706, USA, and Department of Mathematical Sciences, Tsinghua University, Beijing 100084, P.R. China. Email address: jin@math.wisc.edu.

[‡]Department of Mathematical Sciences, Tsinghua University, Beijing 100084, P.R. China. Email address: wenx@mail.tsinghua.edu.cn.

1 Introduction

Hyperbolic systems with geometric source terms arise in many physical applications, including the shallow water equations with bottom topography and the quasi one-dimensional nozzle flow equations with variable cross-sectional area. At the discontinuities of the bottom topography of a river or the cross-sectional area of a nozzle, the source terms have concentrations, corresponding to a δ -function in the source. This reduces the numerical accuracy of a standard shock capturing method for steady state computation, due to the first order numerical viscosity used at the discontinuities [13].

A well adopted strategy for these problems is to design so called *well-balanced* scheme that balances the numerical flux with the source term such that the steady state solution is captured numerically either exactly or with at least a second order accuracy. Many well-balanced schemes have been proposed in recent years, for example the well-balanced scheme based on non-conservative product [13] and its extensions [14], [12], [5], [8], [10], [11], LeVeque's quasi-steady capturing scheme [21], kinetic schemes [4], [23], [2], [30], relaxation schemes [22], [7], central schemes [18], HLLE scheme [6] and schemes based on SGM (surface gradient method) [32], [31]. Nonlinear extension of Roe's linear idea [26] was made in [3], [27], [15]. Most of these methods require the modification of the numerical flux.

In this paper we propose two new well-balanced schemes, which can be applied when a black-box Riemann or approximate Riemann solver is available. A main advantage of these methods are that they do not require the modification of the numerical fluxes for the nonlinear convection terms. Instead, like the interface method of Jin [15], it uses the numerical fluxes rather than cell averages in the source terms. A recent work by the authors [17] was based on this principle. However, this previous work requires the Newton iterations when defining the approximation of the source terms, while the two new methods do not. The first method, called *the mass-energy method*, uses the primitive variable formulation, while the second, called *the complete form method*, integrates the source term into the flux rather than discretizes them separately. These two methods, like the one proposed in [17], are used *only* at cells that contain source term concentrations. In other cells any standard method for regular source terms can be used.

In Sections 2 and 3 we introduce these methods for the shallow water equations and the isothermal nozzle flow equations respectively. The well-balance property of these two methods are shown. Numerical examples demonstrate that these methods give satisfactory unsteady and steady state solutions for subcritical, supercritical and transonic flows. The paper is concluded in Section 4.

In the sequel we will use $x_{j+1/2}$ to denote the grid point, $\Delta x = x_{j+1/2} - x_{j-1/2}$ the mesh size, $w_{j+1/2} = w(x_{j+1/2})$ the interface value of a general quantity w , and $w_j = \frac{1}{\Delta x} \int_{x_{j-1/2}}^{x_{j+1/2}} w(x) dx$ the cell average of w over the cell $[x_{j-1/2}, x_{j+1/2}]$.

2 The shallow water equations

Consider the one-dimensional shallow water equations with topography

$$h_t + (hv)_x = 0, \quad (2.1)$$

$$(hv)_t + (hv^2 + \frac{1}{2}gh^2)_x = -ghB_x, \quad (2.2)$$

where h is the height of the water, v is the mean velocity, g is the gravitational constant, and $B(x)$ is the bottom topograph. The steady state solutions satisfy

$$hv = C_1, \quad (2.3)$$

$$\frac{1}{2}v^2 + gh + gB = C_2. \quad (2.4)$$

These steady state conditions are satisfied not only on smooth part of the solution, but also across a bottom discontinuity [1]. A numerical method for the shallow water equations (2.3), (2.4) is called *well-balanced* [13] if it satisfies the steady state conditions (2.3), (2.4) exactly or with at least a second order accuracy even when the bottom function $B(x)$ contains discontinuities.

2.1 The cell-average method

We first present the conventional *cell average method*,

$$\partial_t h_i + \frac{(hv)_{i+\frac{1}{2}} - (hv)_{i-\frac{1}{2}}}{\Delta x} = 0, \quad (2.5)$$

$$\partial_t (hv)_i + \frac{(hv^2 + \frac{1}{2}gh^2)_{i+\frac{1}{2}} - (hv^2 + \frac{1}{2}gh^2)_{i-\frac{1}{2}}}{\Delta x} = -gh_i \frac{B_{i+\frac{1}{2}} - B_{i-\frac{1}{2}}}{\Delta x}; \quad (2.6)$$

where $B_{i+\frac{1}{2}} = B(x_{i+\frac{1}{2}})$ and the numerical fluxes $(h_{i+1/2}, v_{i+1/2})$ are obtained by a Riemann or approximate Riemann solver for the homogeneous part of equations (2.1), (2.2). Namely, the interface values $h_{i+1/2}$ and $v_{i+1/2}$ are defined by the Godunov or Roe scheme or its higher order extensions.

As is well known, the cell average method is suitable for steady state capturing if the bottom function $B(x)$ is continuous. When $B(x)$ contains a discontinuity, the cell average method generally fails to be well-balanced due to the first order numerical viscosity added at discontinuities. This agrees with the fact that the shallow water equations in the form (2.1), (2.2), which are referred to as the mass-momentum formulation in [1], no longer hold at points where the bottom slope B_x becomes infinite.

The interface methods, to be presented in the next three subsections, are hybrid schemes that use the cell-average method everywhere except at cells that contain a discontinuity of $B(x)$. In the sequel we assume that a discontinuity of $B(x)$ is contained in the middle of a cell $[x_{j-\frac{1}{2}}, x_{j+\frac{1}{2}}]$ for some j .

2.2 An interface method

An interface method was proposed by the authors in [17]:

$$\partial_t h_j + \frac{(hv)_{j+\frac{1}{2}} - (hv)_{j-\frac{1}{2}}}{\Delta x} = 0, \quad (2.7)$$

$$\partial_t (hv)_j + \frac{(hv^2 + \frac{1}{2}gh^2)_{j+\frac{1}{2}} - (hv^2 + \frac{1}{2}gh^2)_{j-\frac{1}{2}}}{\Delta x} = -\frac{g}{\Delta x} \int_{x_{j-\frac{1}{2}}}^{x_{j+\frac{1}{2}}} \hat{h} \hat{B}_x dx; \quad (2.8)$$

where a general hat-function \hat{q} denotes a *smooth function* in cell $[x_{j-\frac{1}{2}}, x_{j+\frac{1}{2}}]$ with endpoint values $q(x_{i\pm\frac{1}{2}})$ at $x_{i\pm\frac{1}{2}}$.

Let $H(x), G(x)$ and $B(x)$, defined in cell $[x_{j-\frac{1}{2}}, x_{j+\frac{1}{2}}]$, to be the *linear interpolant* defined according to

$$H(x_{j\pm\frac{1}{2}}) = (hv)_{j\pm\frac{1}{2}}, \quad G(x_{j\pm\frac{1}{2}}) = \left(\frac{1}{2}v^2 + gh + gB \right)_{j\pm\frac{1}{2}}, \quad \hat{B}(x_{j\pm\frac{1}{2}}) = B_{j\pm\frac{1}{2}}. \quad (2.9)$$

Then \hat{h} and \hat{v} are determined from the identities

$$H \equiv \hat{h}\hat{v}, \quad (2.10)$$

$$G \equiv \frac{1}{2}\hat{v}^2 + g\hat{h} + g\hat{B}, \quad (2.11)$$

or \hat{h} can be determined by solving (numerically)

$$\frac{1}{2} \frac{H^2}{\hat{h}^2} + g\hat{h} + g\hat{B} \equiv G. \quad (2.12)$$

The following theorem shows that above scheme is well-balanced. The proof was given in [17].

Theorem 2.1. *Scheme (2.7), (2.8) can preserve the steady state conditions (2.3)-(2.4) exactly at two sides of the bottom discontinuity:*

$$h_{j-\frac{1}{2}}v_{j-\frac{1}{2}} = h_{j+\frac{1}{2}}v_{j+\frac{1}{2}}, \quad (2.13)$$

$$\frac{1}{2}v_{j-\frac{1}{2}}^2 + gh_{j-\frac{1}{2}} + gB_{j-\frac{1}{2}} = \frac{1}{2}v_{j+\frac{1}{2}}^2 + gh_{j+\frac{1}{2}} + gB_{j+\frac{1}{2}}. \quad (2.14)$$

In practical calculation, one needs to solve \hat{h} from H, G using (2.12). Since \hat{B} is linear, the right hand side of (2.8) is just

$$-g \left(\frac{1}{\Delta x} \int_{x_{j-\frac{1}{2}}}^{x_{j+\frac{1}{2}}} \hat{h} dx \right) \frac{B_{j+\frac{1}{2}} - B_{j-\frac{1}{2}}}{\Delta x}. \quad (2.15)$$

The cell average of \hat{h} in (2.15) was approximated by composite quadrature rules (e.g. the composite Simpson's rule), with the values of \hat{h} at the quadrature points obtained by solving the algebraic equation (2.12) using Newton's method.

In the next two sections, two new interface methods will be presented, both of which can avoid the Newton iterations.

2.3 The mass-energy method

This scheme is based on the mass-energy (or primitive variable) formulation of the shallow water equations:

$$h_t + (hv)_x = 0, \quad (2.16)$$

$$v_t + \left(\frac{1}{2}v^2 + gh + gB\right)_x = 0. \quad (2.17)$$

Near a bottom discontinuity this formulation is assumed to be possibly valid while the original form of shallow water equations (2.1), (2.2) are not valid. A nice feature of this formulation is that the steady state balance (2.3) (2.4) is obviously satisfied if one drops the time derivative. This property is easily preserved at the discrete level by *any* conservative discretization of (2.16), (2.17):

$$\partial_t h_j + \frac{h_{j+\frac{1}{2}}v_{j+\frac{1}{2}} - h_{j-\frac{1}{2}}v_{j-\frac{1}{2}}}{\Delta x} = 0, \quad (2.18)$$

$$\partial_t v_j + \frac{\left(\frac{1}{2}v_{j+\frac{1}{2}}^2 + gh_{j+\frac{1}{2}} + gB_{j+\frac{1}{2}}\right) - \left(\frac{1}{2}v_{j-\frac{1}{2}}^2 + gh_{j-\frac{1}{2}} + gB_{j-\frac{1}{2}}\right)}{\Delta x} = 0. \quad (2.19)$$

It is obvious that this scheme, at steady state, satisfies the discrete balance (2.13) (2.14).

The disadvantage of this method is that it cannot be extended to higher space dimensions.

2.4 The complete form method

This method is also based on (2.7), (2.8). Rewrite (2.8) as

$$\partial_t (hv)_j + \frac{1}{\Delta x} \int_{x_{j-\frac{1}{2}}}^{x_{j+\frac{1}{2}}} E_2 dx = 0 \quad (2.20)$$

where function E_2 , defined in $[x_{j-\frac{1}{2}}, x_{j+\frac{1}{2}}]$, is given by

$$E_2 = (\hat{h}\hat{v}^2)_x + \left(\frac{1}{2}g\hat{h}^2\right)_x + g\hat{h}\hat{B}_x$$

$$\begin{aligned}
&= (\widehat{h\widehat{v}})_x \widehat{v} + (\widehat{h\widehat{v}}) \widehat{v}_x + g\widehat{h}\widehat{h}_x + g\widehat{h}\widehat{B}_x \\
&= H_x \widehat{v} + \widehat{h}(\widehat{v}\widehat{v}_x + g\widehat{h}_x + g\widehat{B}_x) \\
&= H_x \widehat{v} + \widehat{h}G_x;
\end{aligned} \tag{2.21}$$

with H and G given by (2.10), (2.11).

Since $H(x)$ and $G(x)$ are linear functions, one has

$$\begin{aligned}
H_x &= \frac{1}{\Delta x}(H_{j+\frac{1}{2}} - H_{j-\frac{1}{2}}), \\
G_x &= \frac{1}{\Delta x}(G_{j+\frac{1}{2}} - G_{j-\frac{1}{2}}),
\end{aligned}$$

then the values of function E_2 at $x_{j\pm\frac{1}{2}}$ are

$$E_2(x_{j\pm\frac{1}{2}}) = \frac{1}{\Delta x}[(H_{j+\frac{1}{2}} - H_{j-\frac{1}{2}})v_{j\pm\frac{1}{2}} + (G_{j+\frac{1}{2}} - G_{j-\frac{1}{2}})h_{j\pm\frac{1}{2}}]. \tag{2.22}$$

The trapezoidal rule is used to evaluate the cell average of E_2 in (2.20) to yield the following (second order) approximation:

$$\begin{aligned}
&\int_{x_{j-\frac{1}{2}}}^{x_{j+\frac{1}{2}}} E_2 dx \\
&\approx \frac{\Delta x}{2}(E_2(x_{j-\frac{1}{2}}) + E_2(x_{j+\frac{1}{2}})) \\
&= \frac{1}{2} \left[(H_{j+\frac{1}{2}} - H_{j-\frac{1}{2}})(v_{j-\frac{1}{2}} + v_{j+\frac{1}{2}}) + (G_{j+\frac{1}{2}} - G_{j-\frac{1}{2}})(h_{j-\frac{1}{2}} + h_{j+\frac{1}{2}}) \right].
\end{aligned}$$

The complete form method is obtained by using this in (2.20), and (2.7):

$$\partial_t h_j + \frac{(hv)_{j+\frac{1}{2}} - (hv)_{j-\frac{1}{2}}}{\Delta x} = 0, \tag{2.23}$$

$$\begin{aligned}
\partial_t (hv)_j + \frac{1}{2\Delta x} &[(H_{j+\frac{1}{2}} - H_{j-\frac{1}{2}})(v_{j-\frac{1}{2}} + v_{j+\frac{1}{2}}) + (G_{j+\frac{1}{2}} - G_{j-\frac{1}{2}})(h_{j-\frac{1}{2}} + h_{j+\frac{1}{2}})] \\
&= 0;
\end{aligned} \tag{2.24}$$

where the definitions of $H_{j\pm\frac{1}{2}}$ and $G_{j\pm\frac{1}{2}}$ are given in (2.9). This is clearly a second order (in space) discretization of the shallow water equations.

The well-balance property of the complete form scheme (2.23) and (2.24) is easily seen. By dropping the time derivative in (2.23), one immediately gets condition (2.13). Combining this with (2.24) one obtains (2.14) unless $h_{j-\frac{1}{2}} + h_{j+\frac{1}{2}} = 0$ (a dry river).

2.5 The transonic fix

In the transonic case, these two new methods, as the interface method introduced in Section 2.2, need a transonic fix given in [17].

For example, assume $\left| \frac{v_{j-\frac{1}{2}}}{\sqrt{gh_{j-\frac{1}{2}}}} \right| > 1$, $\left| \frac{v_{j+\frac{1}{2}}}{\sqrt{gh_{j+\frac{1}{2}}}} \right| < 1$, and $B_{j-\frac{1}{2}} < B_{j+\frac{1}{2}}$. Let $H_{j+\frac{1}{2}} = h_{j+\frac{1}{2}}v_{j+\frac{1}{2}}$. We choose $h'_{j+\frac{1}{2}}, v'_{j+\frac{1}{2}}$ to satisfy $h'_{j+\frac{1}{2}}v'_{j+\frac{1}{2}} = H_{j+\frac{1}{2}}$ and $|v'_{j+\frac{1}{2}}| = \sqrt{gh'_{j+\frac{1}{2}}}$. Namely, $h'_{j+\frac{1}{2}} = \left(\frac{H_{j+\frac{1}{2}}^2}{g} \right)^{\frac{1}{3}}$ and $v'_{j+\frac{1}{2}} = \frac{H_{j+\frac{1}{2}}}{h'_{j+\frac{1}{2}}}$. Define $G_{j+\frac{1}{2}} = \frac{1}{2}v_{j+\frac{1}{2}}^2 + gh'_{j+\frac{1}{2}} + gB_{j+\frac{1}{2}}$. We also replace the interface values of water height and velocity at $x_{j+\frac{1}{2}}$ by $h'_{j+\frac{1}{2}}, v'_{j+\frac{1}{2}}$.

Other transonic cases are treated similarly.

2.6 Extensions to 2d shallow water equations

In two space dimensions the shallow water equations are given by

$$h_t + (hu)_x + (hv)_y = 0, \quad (2.25)$$

$$(hu)_t + (hu^2 + \frac{1}{2}gh^2)_x + (huv)_y = -ghB_x, \quad (2.26)$$

$$(hv)_t + (huv)_x + (hv^2 + \frac{1}{2}gh^2)_y = -ghB_y, \quad (2.27)$$

where h is the water height, u, v are the velocity in x, y directions respectively and B is the bottom topography, g is the gravitational constant.

In two space dimension one can not derive an algebraic relation like (2.3) and (2.4) for the steady state solution. Therefore we will just extend the 1-d methods to 2d dimension-by-dimension.

For a general quantity q , its two dimensional cell-average value q_{ij} is given by

$$q_{ij} = \frac{1}{\Delta x \Delta y} \int_{x_{i-\frac{1}{2}}}^{x_{i+\frac{1}{2}}} \int_{y_{j-\frac{1}{2}}}^{y_{j+\frac{1}{2}}} q(x, y) dx dy,$$

while the one-dimensional average is defined, for example, by

$$q_{i+\frac{1}{2},j} = \frac{1}{\Delta y} \int_{y_{j-\frac{1}{2}}}^{y_{j+\frac{1}{2}}} q(x_{i+\frac{1}{2}}, y) dy.$$

The cell average method for (2.25)-(2.27) takes the form

$$\begin{aligned} \partial_t h_{ij} + \frac{(hu)_{i+\frac{1}{2},j} - (hu)_{i-\frac{1}{2},j}}{\Delta x} + \frac{(hv)_{i,j+\frac{1}{2}} - (hv)_{i,j-\frac{1}{2}}}{\Delta y} &= 0, \\ \partial_t (hu)_{ij} + \frac{(hu^2 + \frac{1}{2}gh^2)_{i+\frac{1}{2},j} - (hu^2 + \frac{1}{2}gh^2)_{i-\frac{1}{2},j}}{\Delta x} + \frac{(huv)_{i,j+\frac{1}{2}} - (huv)_{i,j-\frac{1}{2}}}{\Delta y} & \end{aligned} \quad (2.28)$$

$$= -gh_{ij} \frac{B_{i+\frac{1}{2},j} - B_{i-\frac{1}{2},j}}{\Delta x}, \quad (2.29)$$

$$\begin{aligned} & \partial_t(hv)_{ij} + \frac{(huv)_{i+\frac{1}{2},j} - (huv)_{i-\frac{1}{2},j}}{\Delta x} + \frac{(hv^2 + \frac{1}{2}gh^2)_{i,j+\frac{1}{2}} - (hv^2 + \frac{1}{2}gh^2)_{i,j-\frac{1}{2}}}{\Delta y} \\ &= -gh_{ij} \frac{B_{i,j+\frac{1}{2}} - B_{i,j-\frac{1}{2}}}{\Delta y}, \end{aligned} \quad (2.30)$$

where the numerical fluxes are given by an (approximate) Riemann solver for the 2d homogeneous shallow water equations.

The extension of the interface method in Section 2.2 is as follows. We will only discuss the discretization of hB_x in (2.26). The discretization of hB_y in (2.27) is similar. If $B(x, y)$ is continuous crossing the line segment between $(x_{i-\frac{1}{2}}, y_j)$ and $(x_{i+\frac{1}{2}}, y_j)$, where $y_j = \frac{1}{2}(y_{j-\frac{1}{2}} + y_{j+\frac{1}{2}})$, we use the standard cell average method (2.29). Assume the discontinuity line of B crosses the line segment between $(x_{k-\frac{1}{2}}, y_l)$ and $(x_{k+\frac{1}{2}}, y_l)$. In the cell centered at (x_k, y_l) , where $x_k = \frac{1}{2}(x_{k-\frac{1}{2}} + x_{k+\frac{1}{2}})$, we replace (2.29) by

$$\begin{aligned} & \partial_t(hu)_{kl} + \frac{(hu^2 + \frac{1}{2}gh^2)_{k+\frac{1}{2},l} - (hu^2 + \frac{1}{2}gh^2)_{k-\frac{1}{2},l}}{\Delta x} + \frac{(huv)_{k,l+\frac{1}{2}} - (huv)_{k,l-\frac{1}{2}}}{\Delta y} \\ &= -g \left(\frac{1}{\Delta x} \int_{x_{k-\frac{1}{2}}}^{x_{k+\frac{1}{2}}} \widehat{h} dx \right) \frac{B_{k+\frac{1}{2},l} - B_{k-\frac{1}{2},l}}{\Delta x}; \end{aligned} \quad (2.31)$$

where as in one dimension, the function \widehat{h}_l is defined together with function \widehat{u}_l by

$$\widehat{h}_l \widehat{u}_l = H, \quad (2.32)$$

$$\frac{1}{2} \widehat{u}_l^2 + g \widehat{h}_l + g \widehat{B}_l = G_l, \quad (2.33)$$

or \widehat{h}_l can be determined by

$$\frac{1}{2} \frac{H_l^2}{\widehat{h}_l} + g \widehat{h}_l + g \widehat{B}_l = G_l \quad (2.34)$$

with functions H_l, G_l, \widehat{B}_l in the interval $[x_{k-\frac{1}{2}}, x_{k+\frac{1}{2}}]$ being linear interpolant determined by

$$H_l(x_{k\pm\frac{1}{2}}) = (hu)_{k\pm\frac{1}{2},l}, \quad G_l(x_{k\pm\frac{1}{2}}) = \left(\frac{1}{2}u^2 + gh + gB \right)_{k\pm\frac{1}{2},l}, \quad \widehat{B}_l(x_{k\pm\frac{1}{2}}) = B_{k\pm\frac{1}{2},l}. \quad (2.35)$$

Numerical integration can be used to evaluate the integral of function \widehat{h}_l in (2.31), with the values of \widehat{h}_l at the quadrature points obtained by solving (2.34) using Newton's iteration, as was done for the 1d problem.

We obtain the interface values of variables h, u in the scheme (2.31) by a Riemann solver for the 1d shallow water equations

$$h_t + (hu)_x = 0, \quad (2.36)$$

$$(hu)_t + (hu^2 + \frac{1}{2}gh^2)_x = 0. \quad (2.37)$$

The interface values of variable v in the scheme (2.31) are still obtained from the 2d Riemann solver. This is natural considering that we only have the energy balance in the one dimensional sense, thus to obtain the constant energy in the x -direction one has to use exactly the 1d solve for h and u based on (2.36), (2.37).

For 2d shallow water equations (2.25)-(2.27), we do not find the proper mass-energy form which can be used to to construct a mass-energy method.

The complete form method for 1d equations can be extended to deal with the 2d equations. Instead of replacing (2.29) by (2.31), we directly use the formula (2.24) to replace the corresponding part in (2.29). We get the following scheme

$$\begin{aligned} \partial_t(hu)_{kj} &+ \frac{1}{2\Delta x} [(H_{k+\frac{1}{2},l} - H_{k-\frac{1}{2},l})(u_{k-\frac{1}{2},l} + u_{k+\frac{1}{2},l}) \\ &+ (G_{k+\frac{1}{2},l} - G_{k-\frac{1}{2},l})(h_{k-\frac{1}{2},l} + h_{k+\frac{1}{2},l})] \\ &+ \frac{(huv)_{k,l+\frac{1}{2}} - (huv)_{k,l-\frac{1}{2}}}{\Delta y} = 0 \end{aligned} \quad (2.38)$$

where $H_{k\pm\frac{1}{2},l}, G_{k\pm\frac{1}{2},l}$ are given by (2.35).

2.7 Numerical examples

In this section, three 1d numerical examples and one 2d example will be given. We use the second order Runge-Kutta time discretization for all the examples. Examples 2.1, 2.2 are Riemann problems from [1] and have been tested in [17]. These two examples are used to test the performance of the two new methods for unsteady solutions of the shallow water equations. Example 2.3 is a test for the steady state solution. These problems will be solved on the domain $[-10, 10]$. For the spatial discretization, we use the Roe solver for the homogeneous shallow water equations with van Leer slope limiter [20]. For the two Riemann problems the zeroth order extrapolation is used as the numerical boundary condition and the "exact" solution is obtained using the complete form method with 1000 cells. In all numerical examples the gravitational constant is set to be 9.8.

Example 2.4 is a 2d Riemann problem used to test the 2d interface method and the complete form method.

Example 2.1: A Riemann problem with solution in the supercritical state. The initial data are given by $(h, v, B) = (4, -10, 0)$ when $x < 0$ and $(h, v, B) = (1, -6, 1)$

when $x > 0$. This is a supercritical case. The energy $\frac{1}{2}v^2 + g(h + B)$ is a constant across the bottom discontinuity at $x = 0$. We use 100 grid points and $\frac{\Delta t}{\Delta x} = 1/20$. The results are plotted in Figure 2.1. One can see that both the mass-energy method and the complete form method give almost identical results, capturing the constant energy across the bottom discontinuity.

There is a spike in the numerical solutions of energy at bottom discontinuity. This spike is a numerical artifact, due to the use of numerical viscosity. This phenomenon was analyzed in [16]. Even with mesh refined, this spike does not disappear. Since the artificial numerical shock layer is not part of the physical solution anyway, this artifact does not effect the other part of the numerical solution. We will give a numerical experiment to test the convergence of our methods in example 2.3.

Example 2.2: A Riemann problem with solution in the transonic state. The initial data are $(h, v, B) = (4, -10, 0)$ when $x < 0$ and $(h, v, B) = (2, 0, 1)$ when $x > 0$. This is a transonic case. The solution reaches the critical state at the right side of the bottom jump, acrossing which the energy $\frac{1}{2}v^2 + g(h + B)$ remains a constant. We use 100 grid points, and take $\frac{\Delta t}{\Delta x} = 1/20$. The numerical solutions are plotted in Figures 2.2. The almost identical results by both schemes correctly predict that the Froude number $(\frac{v}{\sqrt{gh}})$ reaches -1 at the right side of the bottom jump, thanks to the transonic fix used in the methods.

Example 2.3: A steady state calculation. The bottom function is given by

$$B(x) = \begin{cases} 0, & x < -4, \\ 1 + \cos(\frac{\pi x}{8}), & -4 < x < 4, \\ 1, & x > 4, \end{cases}$$

as shown by the dashed line in Figure 2.3. The initial conditions are given by

$$\begin{aligned} h(x, 0) &= 3 - B(x), \\ v(x, 0) &= \frac{2}{h(x, 0)}. \end{aligned}$$

The boundary conditions are given as $hv|_{x=-10} = 2, h|_{x=10} = 2$. We take $\frac{\Delta t}{\Delta x} = 1/10$. Figure 2.4 shows the computed steady state solutions. The results using 100 cells agree well with those using 400 cells and show accurately the constant energy across the bottom discontinuity and sharp resolution of a standing transonic shock.

We can do a numerical experiment to test the convergence property of our methods for this example. At the right of the transonic shock, in the domain $[2, 10]$, the momentum and energy are constant, so the exact steady state solution is known to be subsonic solution of

$$\frac{1}{2}v(x)^2 + g(h(x) + B(x)) = \frac{1}{2} \frac{M_b^2}{h_b^2} + g(h_b + B(10)),$$

$$h(x)v(x) = M_b;$$

where $M_b = 2, h_b = 2$ by the boundary conditions.

Figure 2.5 depicts the errors in the domain $[2, 5]$ between the exact solution and those by the complete form method using different mesh sizes. It can be seen that, near $x = 4$, the numerical solutions converges with a first order accuracy because the bottom is not smooth at $x = 4$. Away from this point, the numerical solutions have a second order accuracy. The results of mass-energy method are similar. Table 1 lists the L^1 -norm of the above mentioned errors by both methods with different mesh sizes. In this table, one can observe the convergence rate of our methods are second order.

Table 1 l^1 -norm of errors of water height in domain $[2, 5]$

errors	the complete form method	the mass-energy method
100 cells	2.043499E-4	2.043498E-4
200 cells	5.275889E-5	5.275921E-5
400 cells	1.337883E-5	1.337907E-5

Table 2 l^1 -norm of errors between different mesh sizes by the complete form method

errors of water height	$[-6, -4.5]$	$[-3.5, 1]$
$h_{100} - h_{200}$	3.401862E-4	8.582698E-5
$h_{200} - h_{400}$	8.758745E-5	2.147203E-5

On the left of the standing transonic shock, we have no exact solution. But we can compare numerical solutions using different mesh sizes to approximate the convergence rate of our methods. Denote by $h_{100}, h_{200}, h_{400}$ solutions of water height obtained using 100, 200, 400 cells respectively. Table 2 lists the l^1 -norm of $h_{100} - h_{200}, h_{200} - h_{400}$ by the complete form method in domain $[-6, -4.5]$ and $[-3.5, 1]$ respectively. The mass-energy method gives nearly the same results. This table shows the second order accuracy of our methods in these domains. These numerical experiments show that, although our methods may reduce to the first order accuracy at points where the bottom or solution is not smooth, or even produce a spike near

the bottom discontinuity, they do capture the steady state solution with second order accuracy in the domain where the bottom and solution are smooth.

Example 2.4: A 2d Riemann problem. We consider a 2d Riemann problem with a discontinuous bottom. The initial data are $(h, u, v, B) = (15, -0.1, 0.1, 0)$ when $(x, y) \in [0, 100] \times [100, 200]$ and $(h, u, v, B) = (10, -0.1, 0.1, 10)$ elsewhere. The solution of this problem describes the motion of water outside the square $[0, 100] \times [100, 200]$ into this region across the bottom discontinuous line. The problem is solved in the square $(x, y) \in [0, 200] \times [0, 200]$. A uniform space mesh is used, and $\frac{\Delta t}{\Delta x} = \frac{\Delta t}{\Delta y} = 1/20$.

One of the main difficulties for the 2d problem with a discontinuous bottom is that there are no analytic solutions available. One reasonable approach is to smooth out the bottom by replacing the discontinuous B with a continuous function connecting both sides of the discontinuity through a narrow transition zone. The standard cell average method will be used to solve this regularized problem by putting enough grid points inside the transition zone of the smoothed bottom. As one makes the transition zone narrower and narrower, the converged solution (if exists) will be defined as the solution to the problem with a discontinuous bottom. Results so obtained will serve the purpose of the "exact" solution, and will be tested against the numerical solutions computed using the original discontinuous bottom.

We have tested this "infinite slope limit" idea for the 1d Riemann problem Example 2.1. The limiting solution seems to coincide with the solution with the discontinuous bottom. Therefore, we will adopt this approach for the 2d example.

The numerical flux for the cell average method used in cells with continuous bottom function is based on the Roe solver for 2d shallow water equations [28]. Figure 2.6 shows the water height at $t = 4$ computed by the cell average method along with the bottom function smoothed by a linear function. The computation was carried out on an 100×100 cells, with five cells inside the transition zone of the smoothed bottom function.

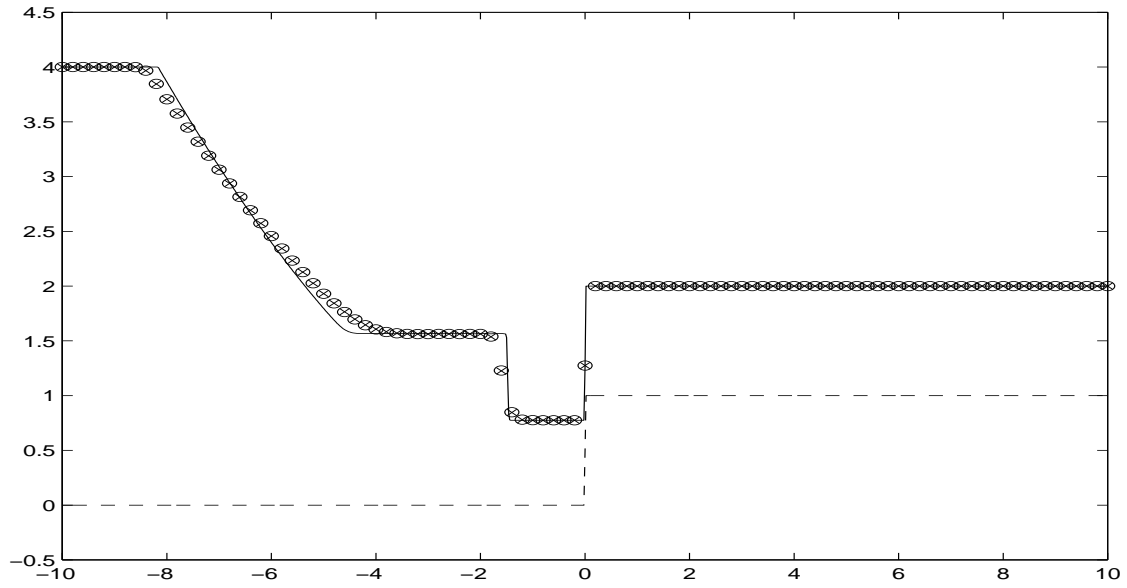
We test the behavior of the 2d interface method and the 2d complete form method.

Figures 2.7 draws respectively the water height and energy in x -direction ($\frac{1}{2}u^2 + g(h + B)$) at $t = 4$ by the 2d complete form method using 100×100 cells.

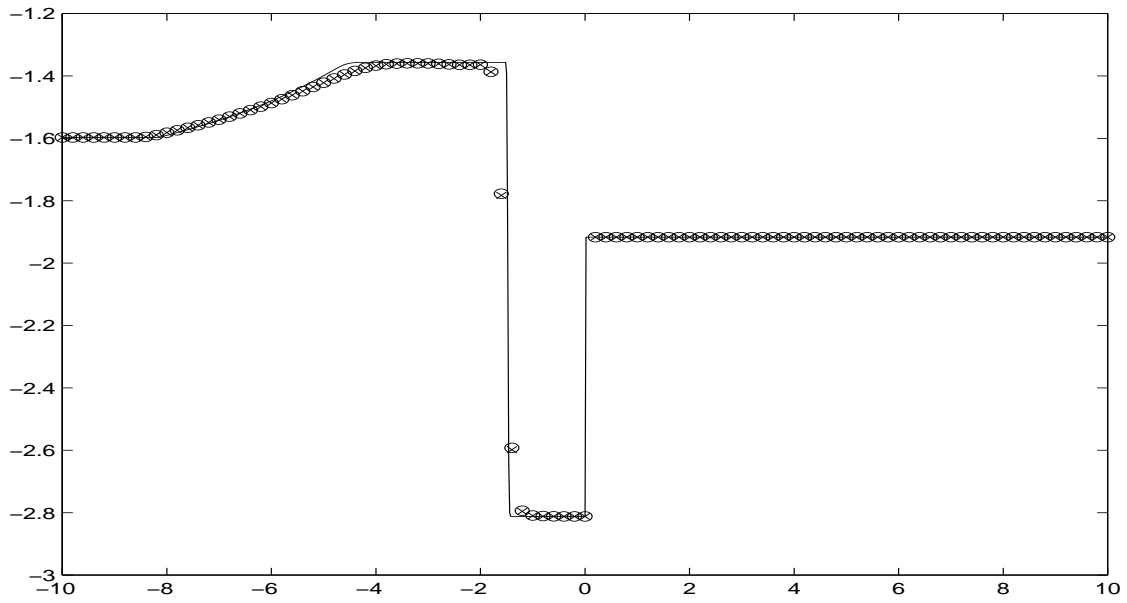
In Figures 2.8-2.9, we compare the numerical solutions at $t = 4$ by the cell average method with smoothed bottoms with those by the 2d complete form method. The solutions to be compared with are the water height and energy in x direction at $y = 120$. One can see that the solutions by the two methods using 400×400 cells are all similar. But on the 100×100 mesh, the complete form method gives better numerical resolutions across the bottom jump than the cell average method that uses the smoothed bottom function. This is not surprising since the smoothed bottom idea is similar to the idea of artificial viscosity in shock capturing. Another observation from these computations is that the energy in the direction normal to the discontinuous line is a constant across the discontinuity.

We have also used the 2d interface method for this problem. The results are

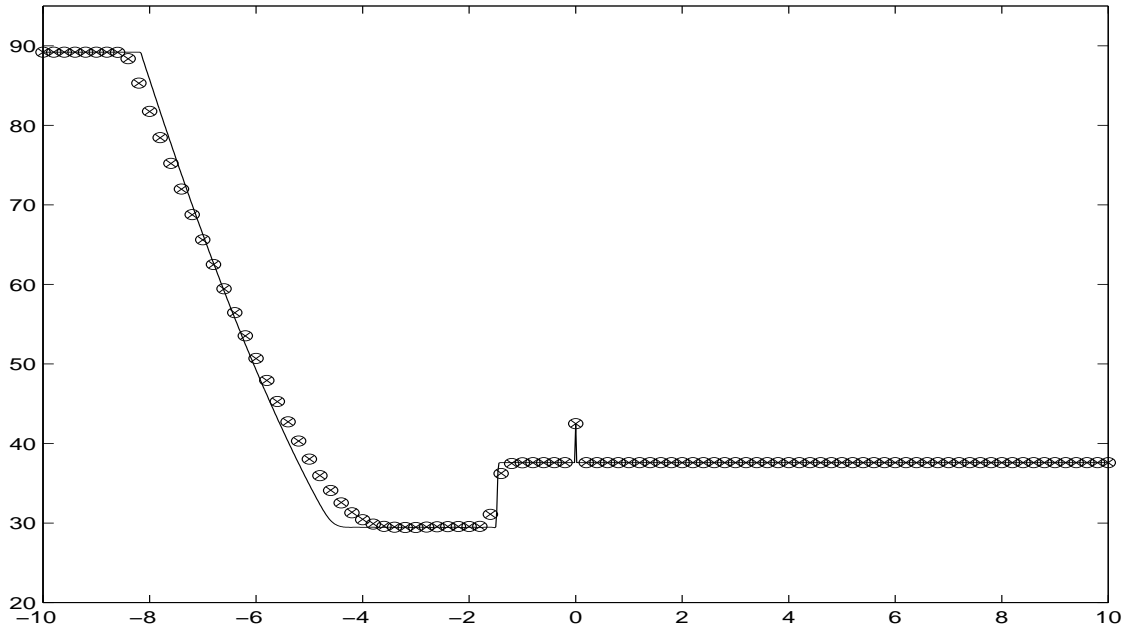
almost the same as the complete form method, thus will not be reported here.



(a): water height (dashed line represents the bottom).

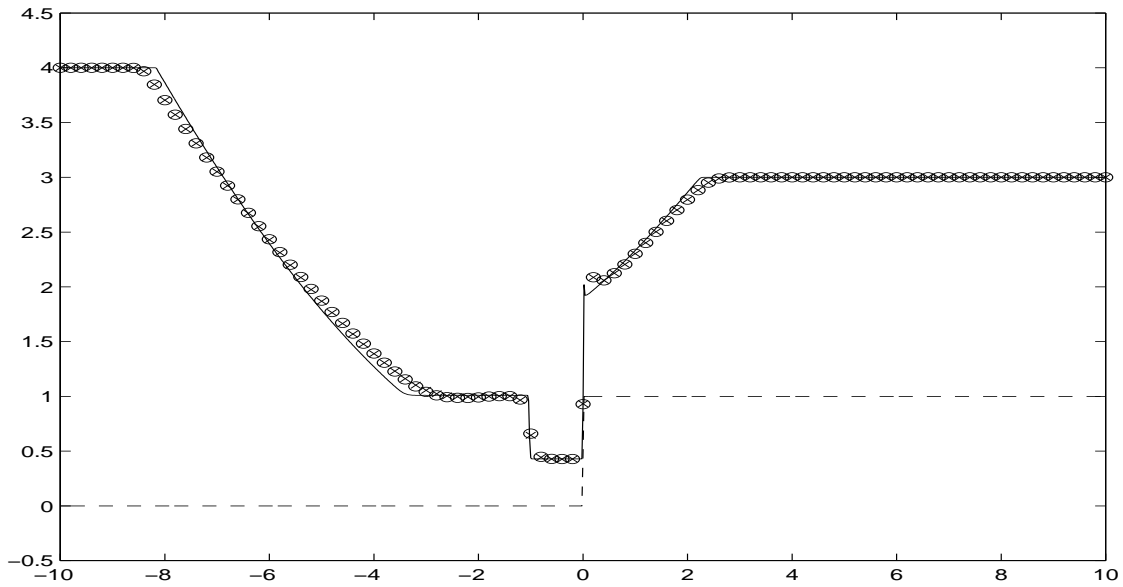


(b): Froude number $\frac{v}{\sqrt{gh}}$.

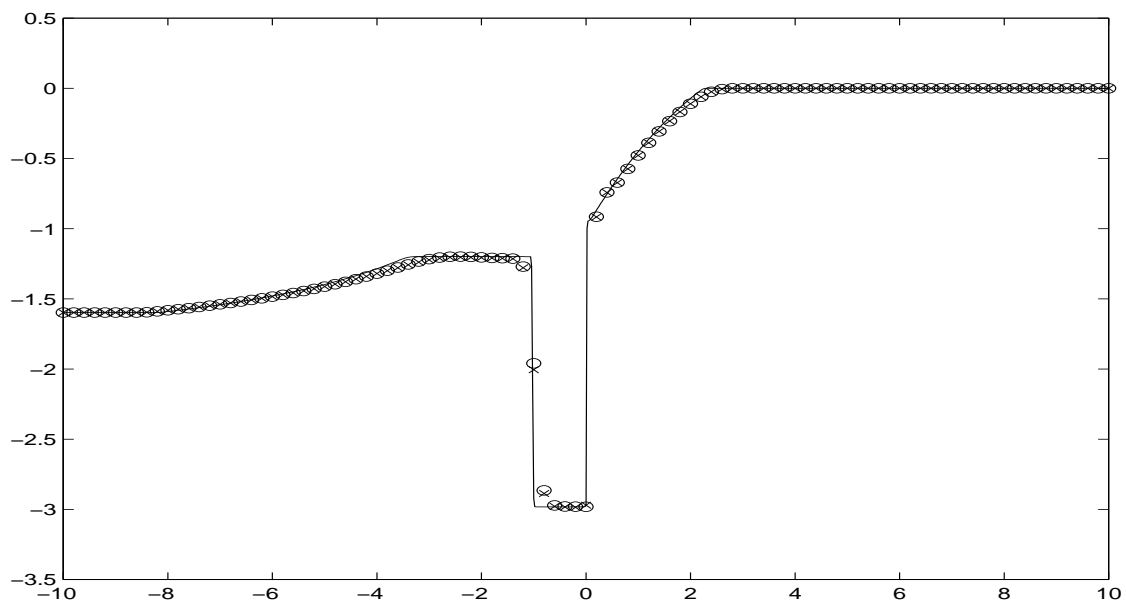


(c): Energy.

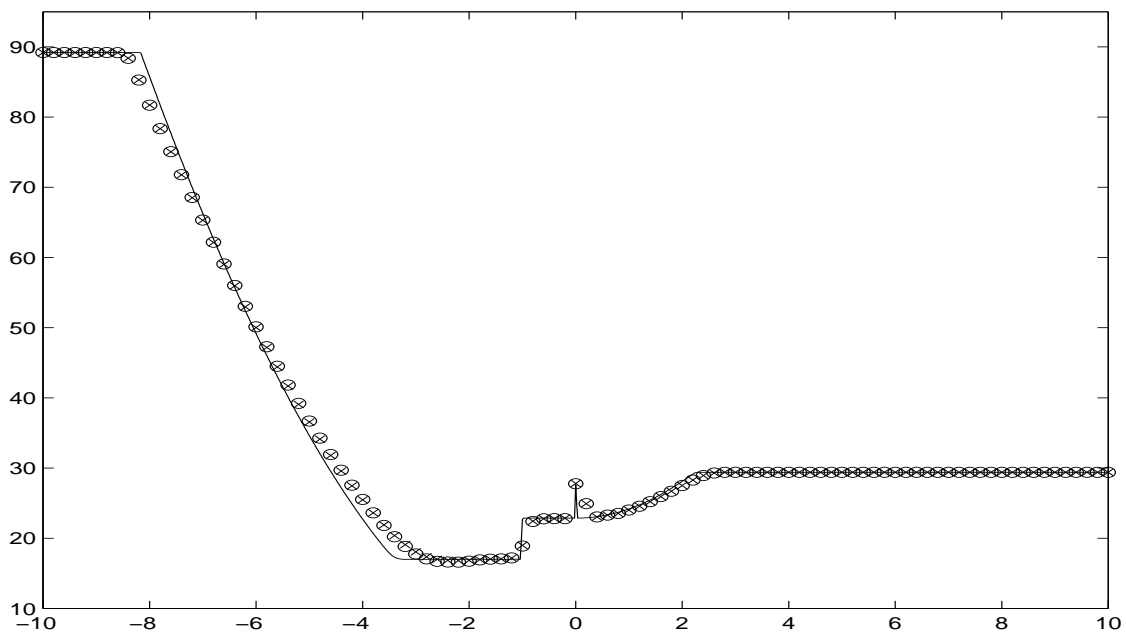
Figure 2.1 Example 2.1, the supercritical case. Solutions at $t = 0.5$. Solid line: the exact solution; "o": the solution by the mass-energy method using 100 cells; "x": the solution by the complete form method using 100 cells.



(a): water height (dashed line represents the bottom).



(b): Froude number.



(c): Energy.

Figure 2.2 Example 2.2, the transonic case. $t=0.5$. Solid line: the exact solution; "o": the solution by the mass-energy method using 100 cells; "x": the solution by the complete form method using 100 cells.

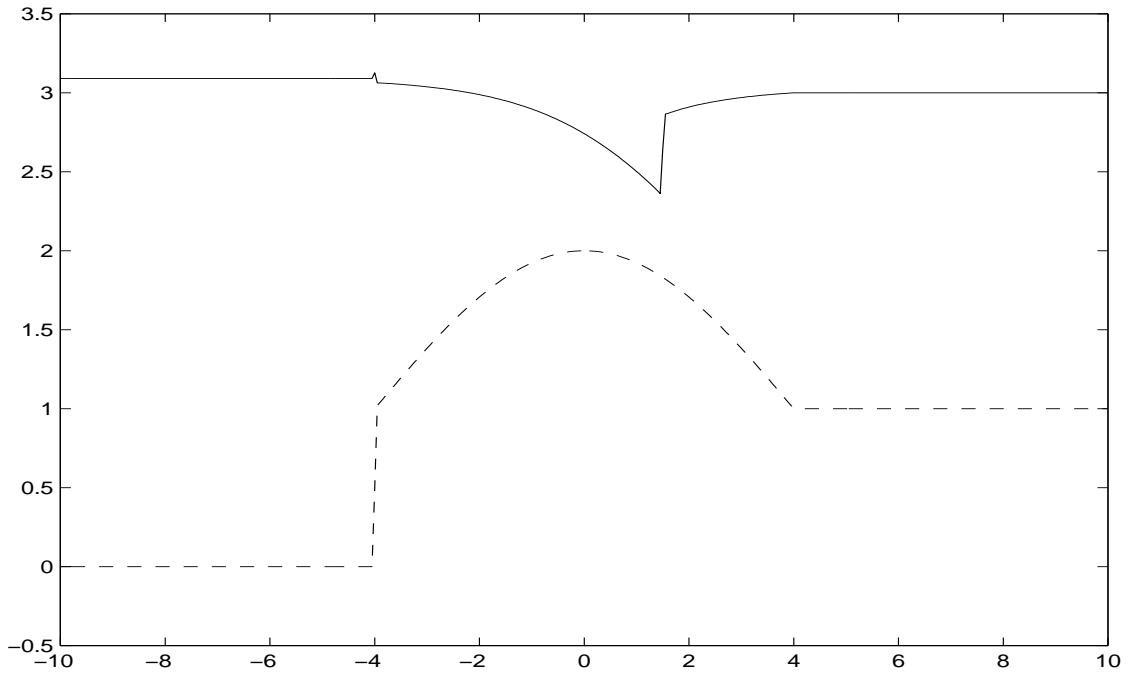
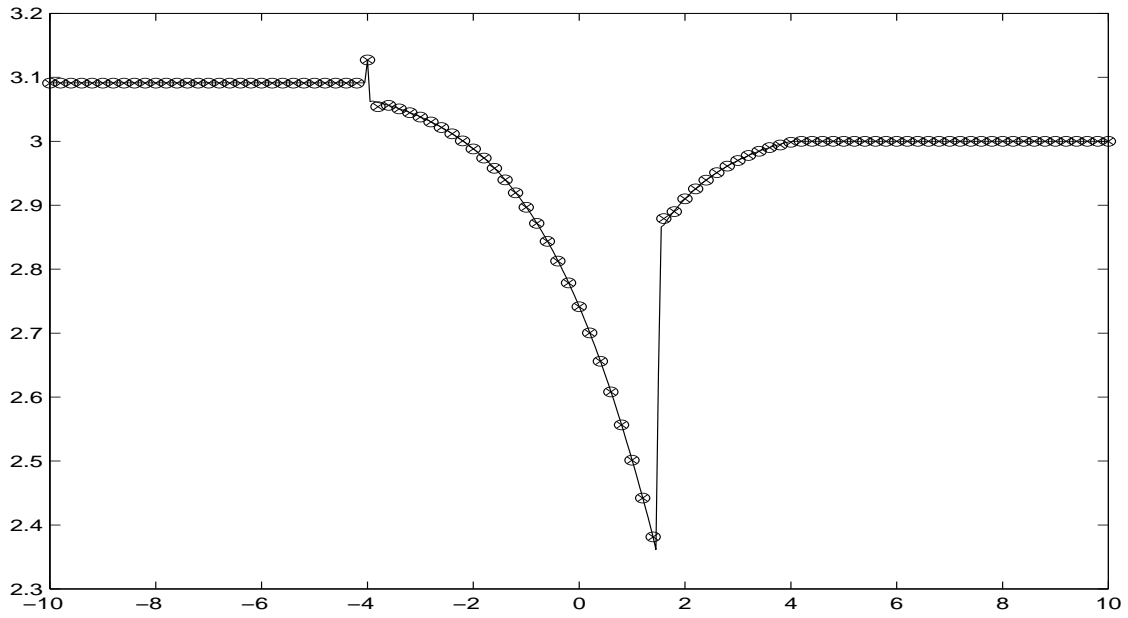
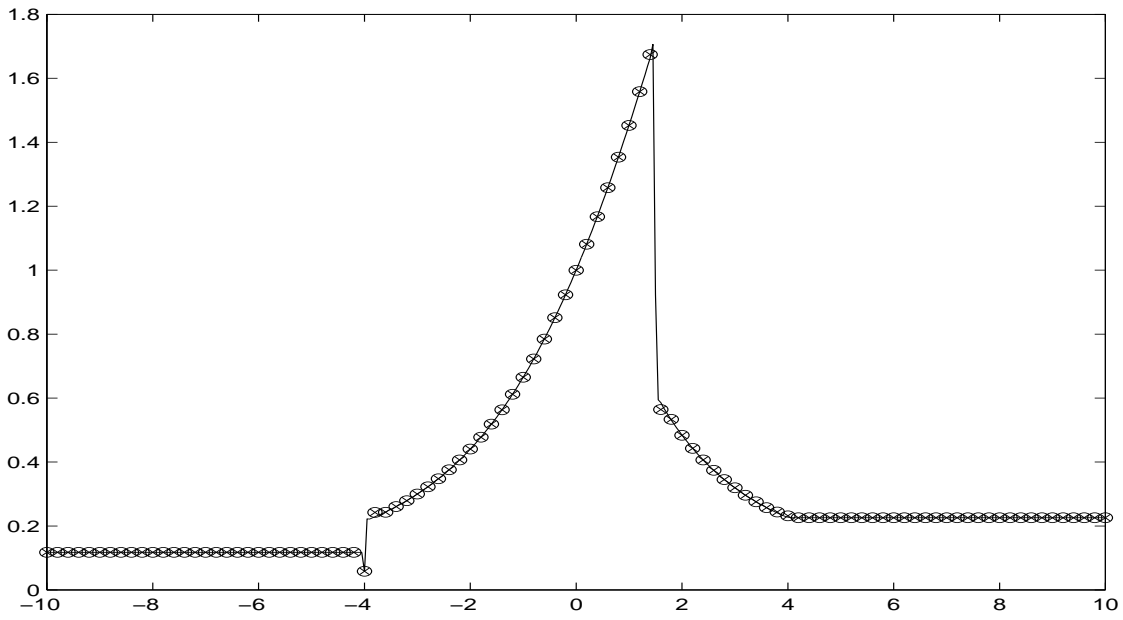


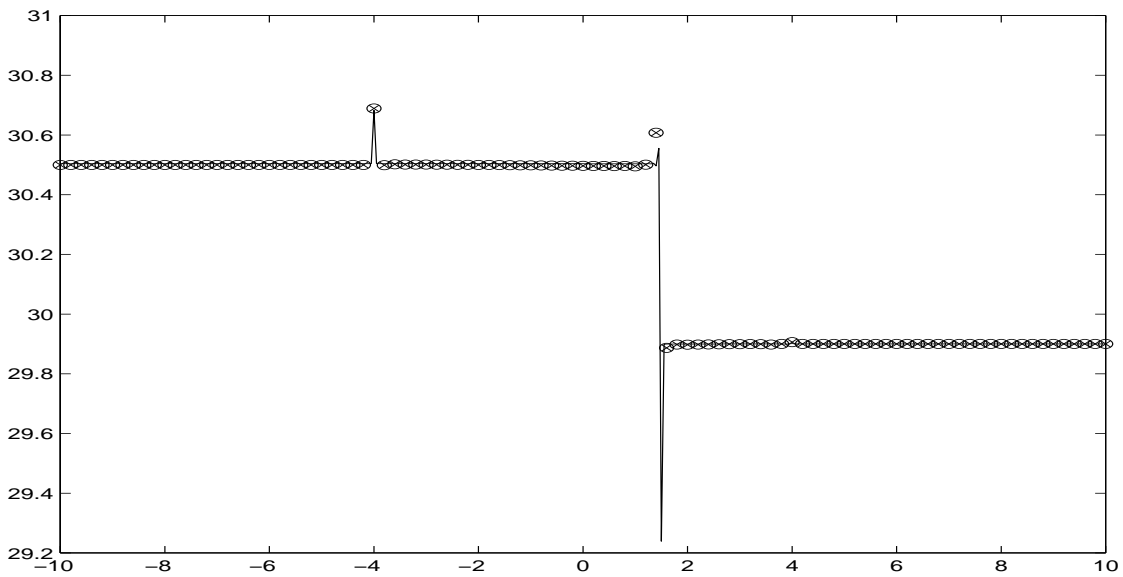
Figure 2.3 Example 2.3. Water height at steady state along with the bottom topography; solid line: water surface; dashed line: bottom function $B(x)$.



(a): water height.



(b): Froude number.



(c): energy.

Figure 2.4 Example 2.3. Steady state solutions. Solid line: solution of the complete form method using 400 cells; "o": solution of the complete form method using 100 cells; "x": solution of the mass-energy method using 100 cells.

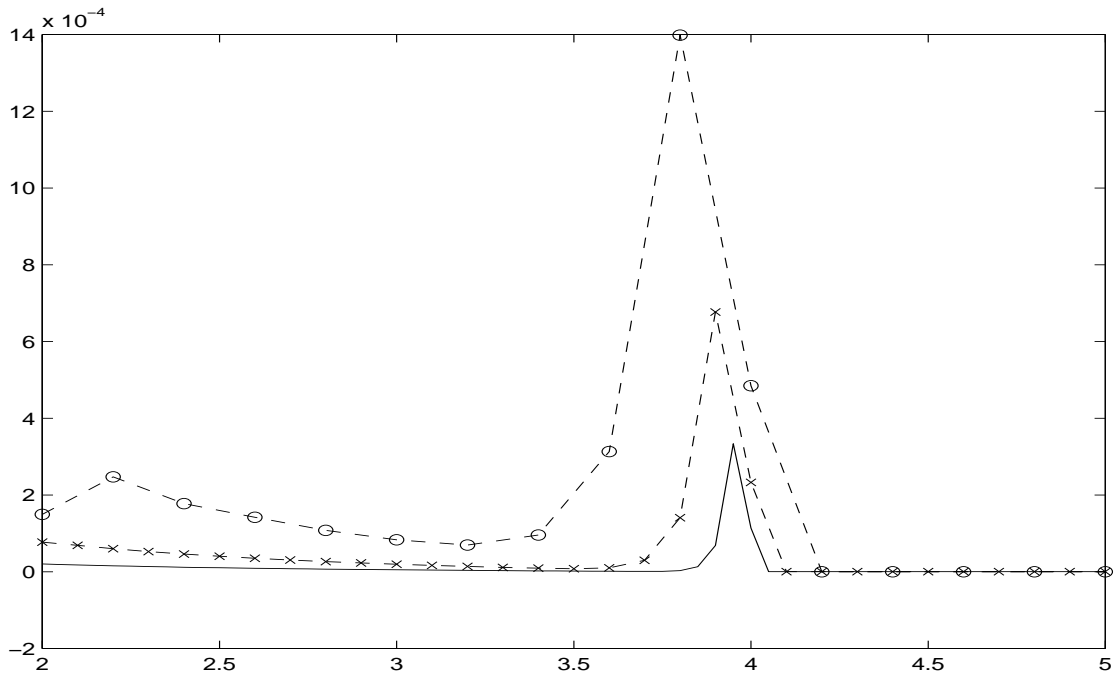


Figure 2.5 Example 2.3. Errors between numerical water height and the exact solution by the complete form method in domain $[2, 5]$; "o": 100 cells; "x": 200 cells; solid line: 400 cells.

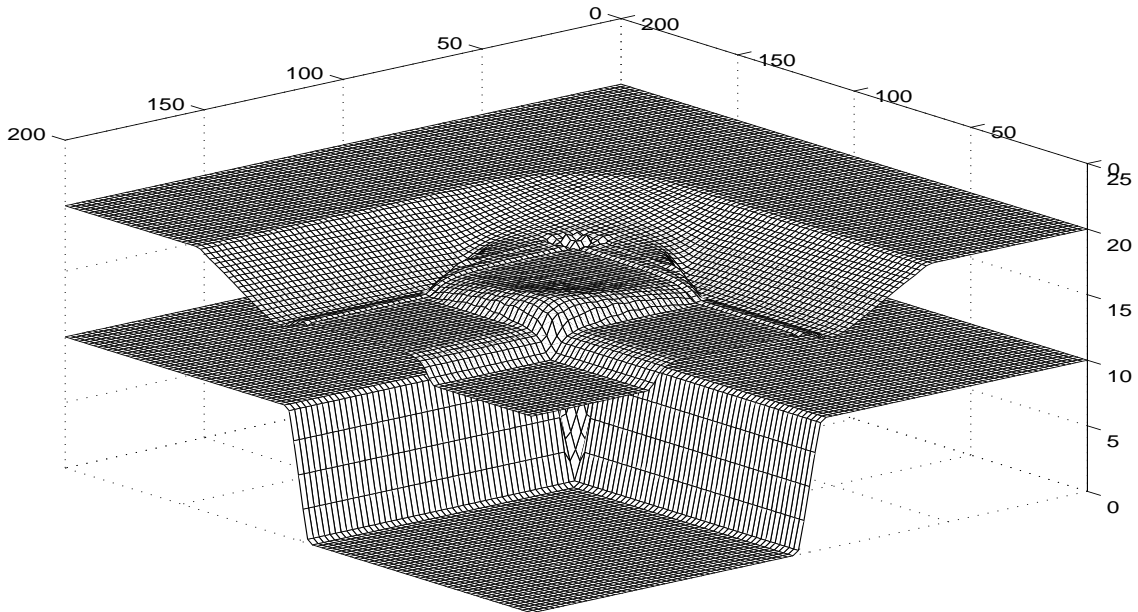
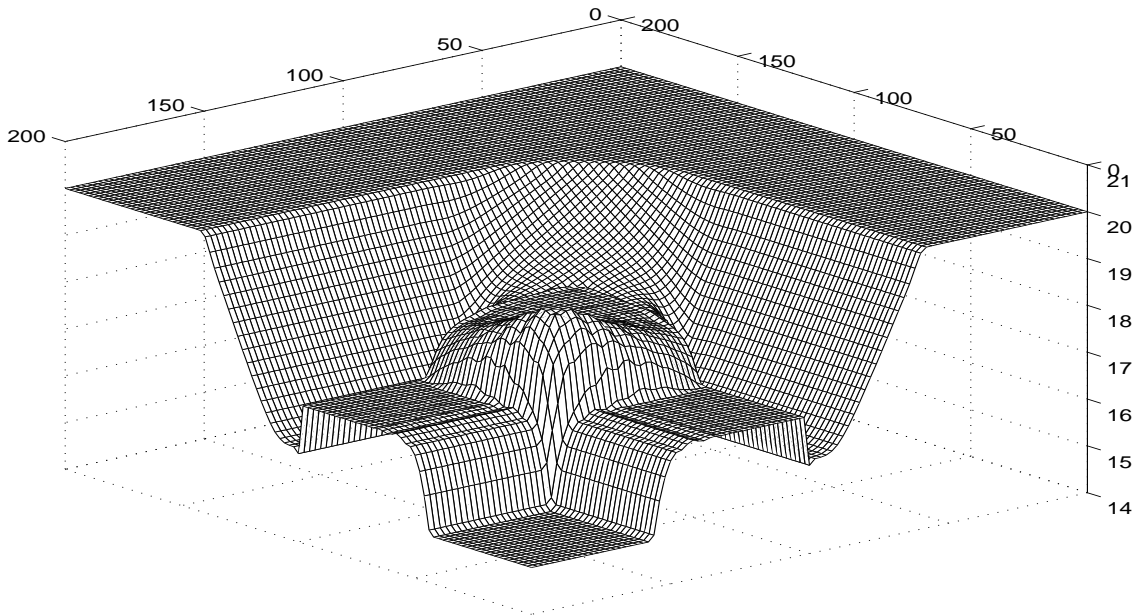
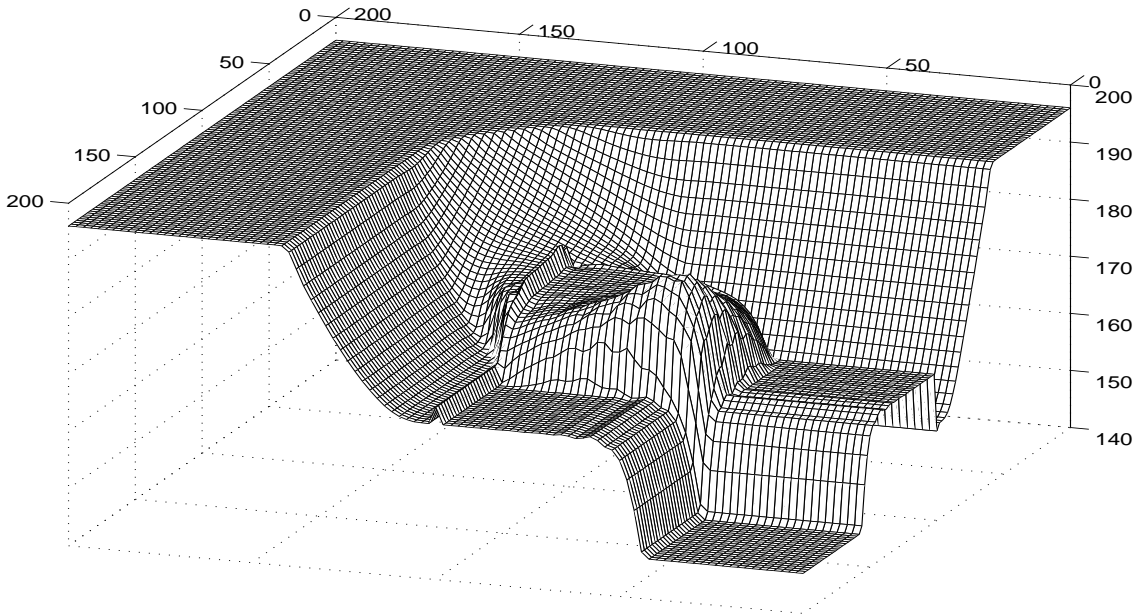


Figure 2.6 Example 2.4, a 2d Riemann problem. Upper surface: water height at $t=4$ by the cell average method using a smoothed bottom function with 100×100 cells; lower surface: the smoothed bottom function.

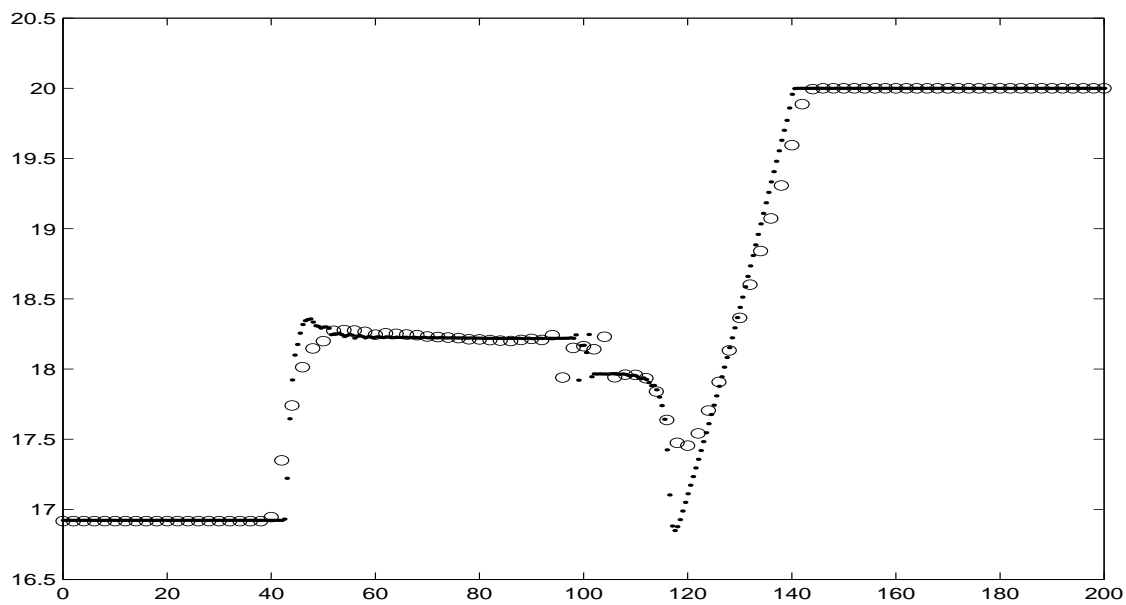


(a): water height.

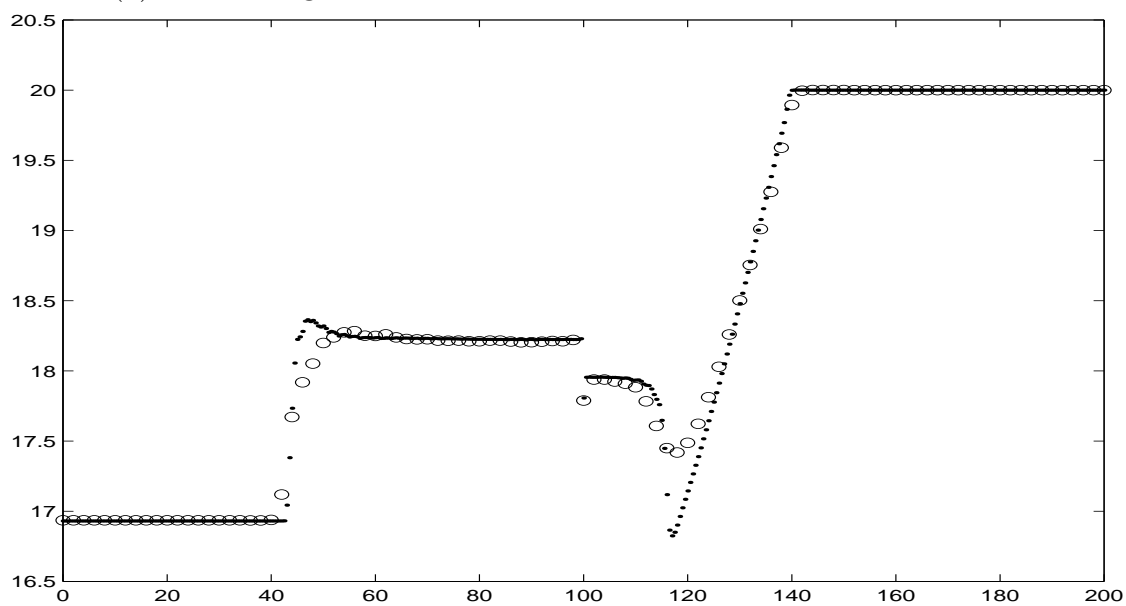


(b): Energy in x direction.

Figure 2.7 Example 2.4, a 2d Riemann problem. Numerical solutions at $t=4$ by the 2d complete form method using 100×100 cells.

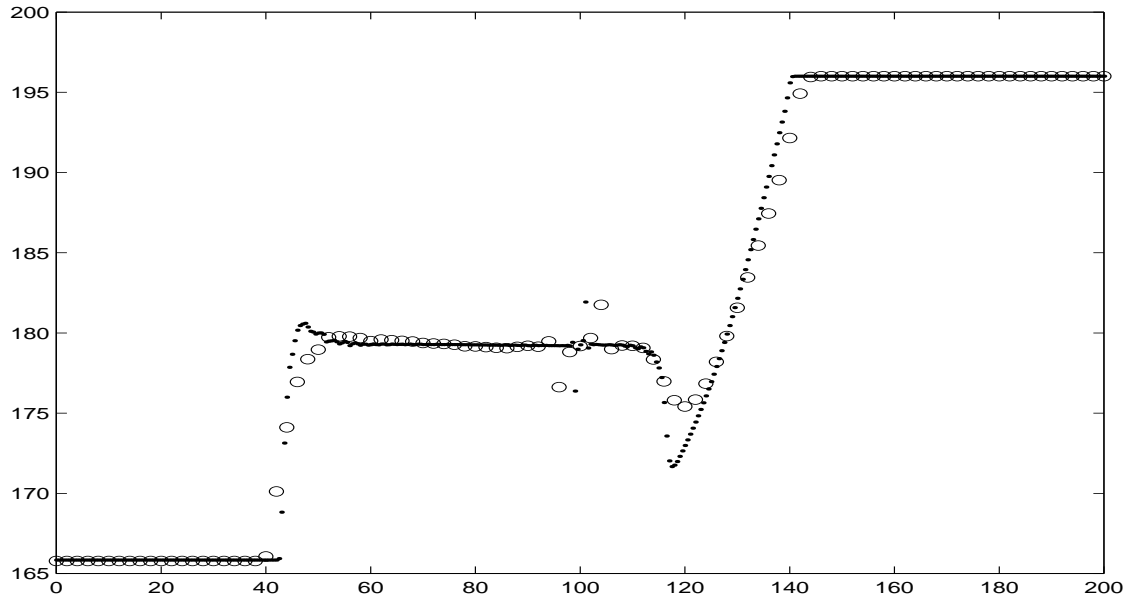


(a): cell average method with a smoothed bottom function.

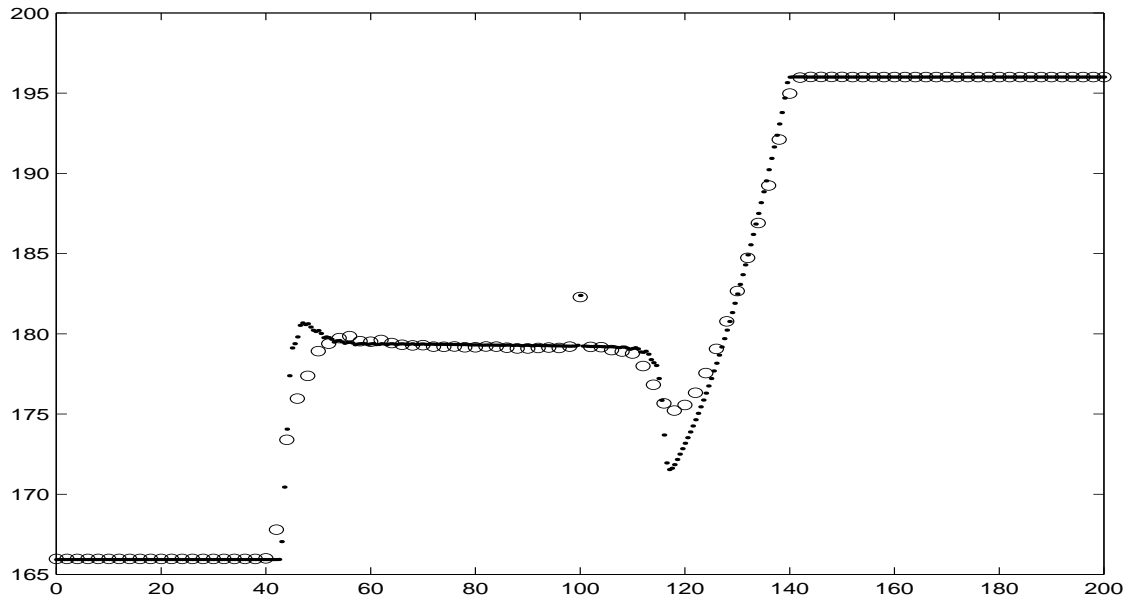


(b): The complete form method.

Figure 2.8 Example 2.4, a 2d Riemann problem. Water height at $t=4, y=120$.
 ".": solution using 400×400 cells; "o": solution using 100×100 cells.



(a): cell average method with a smoothed bottom function.



(b): The complete form method.

Figure 2.9 Example 2.4, a 2d Riemann problem. Energy at $t=4$, $y=120$. ".": solution using 400×400 cells; "o": solution using 100×100 cells.

3 The isothermal nozzle flow equations

Consider the system describing the evolution of an isothermal fluid in a nozzle

$$\partial_t(a\rho) + \partial_x(a\rho v) = 0, \quad (3.39)$$

$$\partial_t(a\rho v) + \partial_x(a\rho v^2 + k a \rho^\gamma) = p(\rho) \partial_x a; \quad (3.40)$$

where ρ, v represent density and velocity of the fluid, $a(x) > 0$ is the cross-sectional area, $p(\rho)$ is the pressure given by the relation

$$p(\rho) = k\rho^\gamma.$$

Equations (3.39), (3.40) reduce to the standard isentropic equations when $a(x)$ is constant.

When the steady state solutions are smooth, they satisfy

$$a\rho v = C_1, \quad (3.41)$$

$$\frac{1}{2}v^2 + k\frac{\gamma}{\gamma-1}\rho^{\gamma-1} = C_2. \quad (3.42)$$

Furthermore, these steady state conditions also hold across a cross-sectional discontinuity [19].

The cell average method for the isothermal nozzle flow equations takes the form

$$\partial_t(a\rho)_i + \frac{(a\rho v)_{i+\frac{1}{2}} - (a\rho v)_{i-\frac{1}{2}}}{\Delta x} = 0, \quad (3.43)$$

$$\partial_t(a\rho v)_i + \frac{(a\rho v^2 + ka\rho^\gamma)_{i+\frac{1}{2}} - (a\rho v^2 + ka\rho^\gamma)_{i-\frac{1}{2}}}{\Delta x} = k\rho_i^\gamma \frac{a_{i+\frac{1}{2}} - a_{i-\frac{1}{2}}}{\Delta x}, \quad (3.44)$$

where the fluxes are obtained by an (approximate) Riemann solver for the homogeneous part of equations (3.39), (3.40).

Assume a cross-sectional discontinuity is contained in the middle of the cell $[x_{j-\frac{1}{2}}, x_{j+\frac{1}{2}}]$ for some j . The interface method in [17] in this cell takes the form

$$\partial_t(a\rho)_j + \frac{(a\rho v)_{j+\frac{1}{2}} - (a\rho v)_{j-\frac{1}{2}}}{\Delta x} = 0, \quad (3.45)$$

$$\partial_t(a\rho v)_j + \frac{(a\rho v^2 + ka\rho^\gamma)_{j+\frac{1}{2}} - (a\rho v^2 + ka\rho^\gamma)_{j-\frac{1}{2}}}{\Delta x} = \frac{k}{\Delta x} \int_{x_{j-\frac{1}{2}}}^{x_{j+\frac{1}{2}}} \widehat{\rho}^\gamma \widehat{a}_x dx; \quad (3.46)$$

where a general hat-function \widehat{q} denotes a *smooth function* in cell $[x_{j-\frac{1}{2}}, x_{j+\frac{1}{2}}]$ with endpoint values $q(x_{j\pm\frac{1}{2}})$ at $x_{j\pm\frac{1}{2}}$.

In [17], the function \widehat{a} was chosen to be the linear interpolant of $a_{j\pm\frac{1}{2}}$ at $x_{j\pm\frac{1}{2}}$. The functions $\widehat{\rho}, \widehat{v}$ are determined from the algebraic relation

$$\widehat{a}\widehat{\rho}\widehat{v} = H, \quad (3.47)$$

$$\frac{1}{2}\widehat{v}^2 + k\frac{\gamma}{\gamma-1}\widehat{\rho}^{\gamma-1} = G, \quad (3.48)$$

with functions H, G in the cell $[x_{j-\frac{1}{2}}, x_{j+\frac{1}{2}}]$ to be linear functions satisfying

$$H(x_{j\pm\frac{1}{2}}) = (a\rho v)_{j\pm\frac{1}{2}}, \quad G(x_{j\pm\frac{1}{2}}) = \left(\frac{1}{2}v^2 + k\frac{\gamma}{\gamma-1}\rho^{\gamma-1} \right)_{j\pm\frac{1}{2}}. \quad (3.49)$$

To evaluate the integral in (3.46), the same numerical strategy as for the shallow water equations was used.

3.1 The mass-energy method and the complete form method

As for the shallow water equations, we can also design the mass-energy method and the complete form method for the isothermal nozzle flow, both of which avoid the Newton iteration.

The isothermal nozzle flow equations (3.39), (3.40) have the mass-energy form

$$\partial_t(a\rho) + \partial_x(a\rho v) = 0, \quad (3.50)$$

$$\partial_t v + \partial_x \left(\frac{1}{2}v^2 + k\frac{\gamma}{\gamma-1}\rho^{\gamma-1} \right) = 0. \quad (3.51)$$

The mass-energy method based on (3.50), (3.51) in the cell $[x_{j-\frac{1}{2}}, x_{j+\frac{1}{2}}]$ is the standard finite volume discretization

$$\partial_t(a\rho)_j + \frac{(a\rho v)_{j+\frac{1}{2}} - (a\rho v)_{j-\frac{1}{2}}}{\Delta x} = 0 \quad (3.52)$$

$$\partial_t v_j + \frac{\left(\frac{1}{2}v^2 + k\frac{\gamma}{\gamma-1}\rho^{\gamma-1} \right)_{j+\frac{1}{2}} - \left(\frac{1}{2}v^2 + k\frac{\gamma}{\gamma-1}\rho^{\gamma-1} \right)_{j-\frac{1}{2}}}{\Delta x} = 0. \quad (3.53)$$

To design the complete form method, we rewrite (3.46) into the complete form

$$\partial_t(a\rho v)_j + \frac{1}{\Delta x} \int_{x_{j-\frac{1}{2}}}^{x_{j+\frac{1}{2}}} E_2 dx = 0, \quad (3.54)$$

with function E_2 defined in $[x_{j-\frac{1}{2}}, x_{j+\frac{1}{2}}]$ by

$$\begin{aligned} E_2 &= (\widehat{a\rho v^2})_x + (k\widehat{a\rho^\gamma})_x - k\widehat{\rho^\gamma a}_x \\ &= (\widehat{a\rho v})_x \widehat{v} + (\widehat{a\rho v}) \widehat{v}_x + k\gamma \widehat{a\rho^{\gamma-1}} \widehat{\rho}_x \\ &= H_x \widehat{v} + \widehat{a\rho} \left[\widehat{v v}_x + k\frac{\gamma}{\gamma-1} (\widehat{\rho^{\gamma-1}})_x \right] \\ &= H_x \widehat{v} + \widehat{a\rho} G_x. \end{aligned} \quad (3.55)$$

As in the shallow water case, we use the trapezoidal rule to evaluate the integral of function E_2 in the cell $[x_{j-\frac{1}{2}}, x_{j+\frac{1}{2}}]$,

$$\begin{aligned} & \int_{x_{j-\frac{1}{2}}}^{x_{j+\frac{1}{2}}} E_2 dx \\ & \approx \frac{\Delta x}{2} (E_2(x_{j-\frac{1}{2}}) + E_2(x_{j+\frac{1}{2}})) \\ & = \frac{1}{2} [(H_{j+\frac{1}{2}} - H_{j-\frac{1}{2}})(v_{j-\frac{1}{2}} + v_{j+\frac{1}{2}}) + (G_{j+\frac{1}{2}} - G_{j-\frac{1}{2}})(a_{j-\frac{1}{2}}\rho_{j-\frac{1}{2}} + a_{j+\frac{1}{2}}\rho_{j+\frac{1}{2}})] \end{aligned}$$

with definitions of $H_{j\pm\frac{1}{2}}, G_{j\pm\frac{1}{2}}$ given by (3.49).

The complete form method, defined in the cell $[x_{j-\frac{1}{2}}, x_{j+\frac{1}{2}}]$ is then

$$\partial_t(a\rho) + \partial_x(a\rho v) = 0, \quad (3.56)$$

$$\begin{aligned} \partial_t(a\rho v)_j + \frac{1}{2\Delta x} [(H_{j+\frac{1}{2}} - H_{j-\frac{1}{2}})(v_{j-\frac{1}{2}} + v_{j+\frac{1}{2}}) \\ + (G_{j+\frac{1}{2}} - G_{j-\frac{1}{2}})(a_{j-\frac{1}{2}}\rho_{j-\frac{1}{2}} + a_{j+\frac{1}{2}}\rho_{j+\frac{1}{2}})] = 0. \end{aligned} \quad (3.57)$$

For isothermal nozzle flow equations, both two methods are able to handle the transonic problems well *without* any transonic fix.

3.2 Numerical examples

We now use numerical examples to test the two new methods for both unsteady and steady state calculations for the isothermal nozzle flow equations. The second order Runge-Kutta method is used for the time discretization in all examples. We choose $k = 1, \gamma = 4/3$ in the computation. Below all the examples are solved numerically on the domain $[-6, 6]$.

Example 3.1 is a Riemann problem studied in [19] and tested by our previous interface method in [17]. We use the Godunov solver for numerical flux in this problem, since the density is low and the Roe solver will encounter problems [24]. The zeroth order extrapolation boundary condition is used. We take $\frac{\Delta t}{\Delta x} = 1/5$. The "exact" solution is obtained by the complete form method using 1000 spatial cells. Example 3.2 is used to test the schemes' ability to capture the steady state solution. For spatial discretization, we use the Roe solver for numerical fluxes in equations (3.39)-(3.40) (for the reason we choose Roe over Godunov see the Remark below).

Example 3.1. A Riemann problem with solution in both the super- and sub-sonic states. The initial data are $(\rho, v, a) = (4, -1.6, 1.5)$ when $x < 0$ and $(\rho, v, a) = (6, 1, 2.5)$ when $x > 0$. This is a mixed sub- and super-sonic case. The energy $\frac{1}{2}v^2 + k\frac{\gamma}{\gamma-1}\rho^{\gamma-1}$ is equal on both sides of the cross-sectional discontinuity. The numerical solutions using 100 cells along with the "exact" solution are shown in Figure 3.1. Our solutions yield the constant numerical energy at two sides of cross-sectional jump.

Example 3.2. A steady state problem. The cross-sectional area function is given by

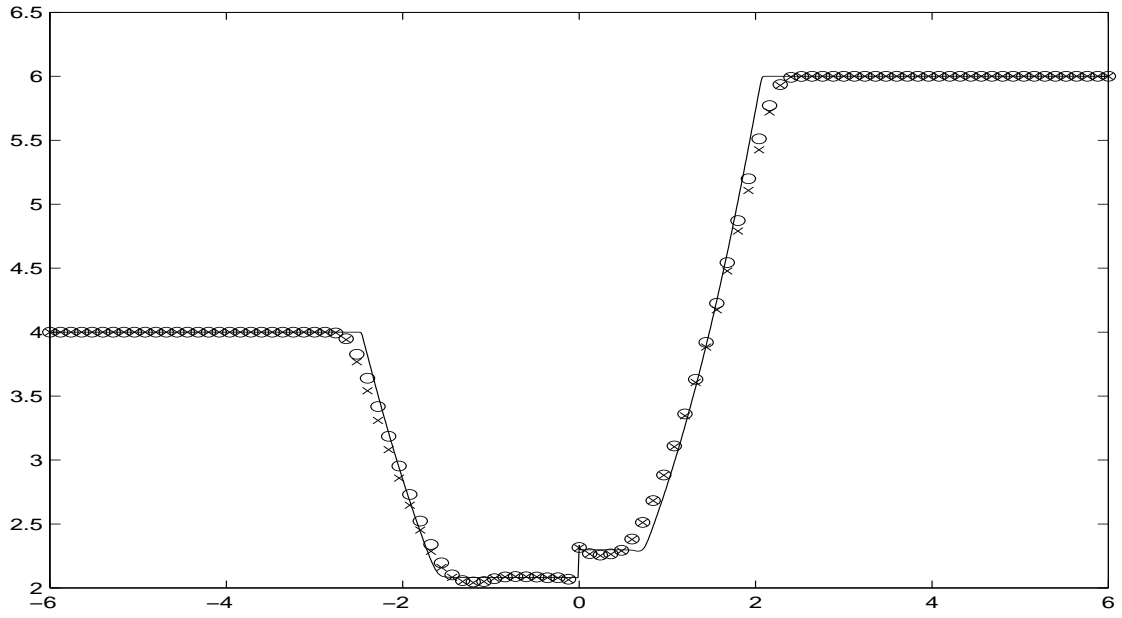
$$a(x) = \begin{cases} 2, & x < -2, \\ 2 + \frac{1}{2} \cos\left(\frac{\pi x}{4}\right), & -2 < x < 0, \\ 2.5 + \frac{1}{2} \cos\left(\frac{\pi x}{6}\right), & 0 < x < 3, \\ 2.5, & x > 3, \end{cases}$$

as shown in the Figure 3.2. The initial conditions are given by

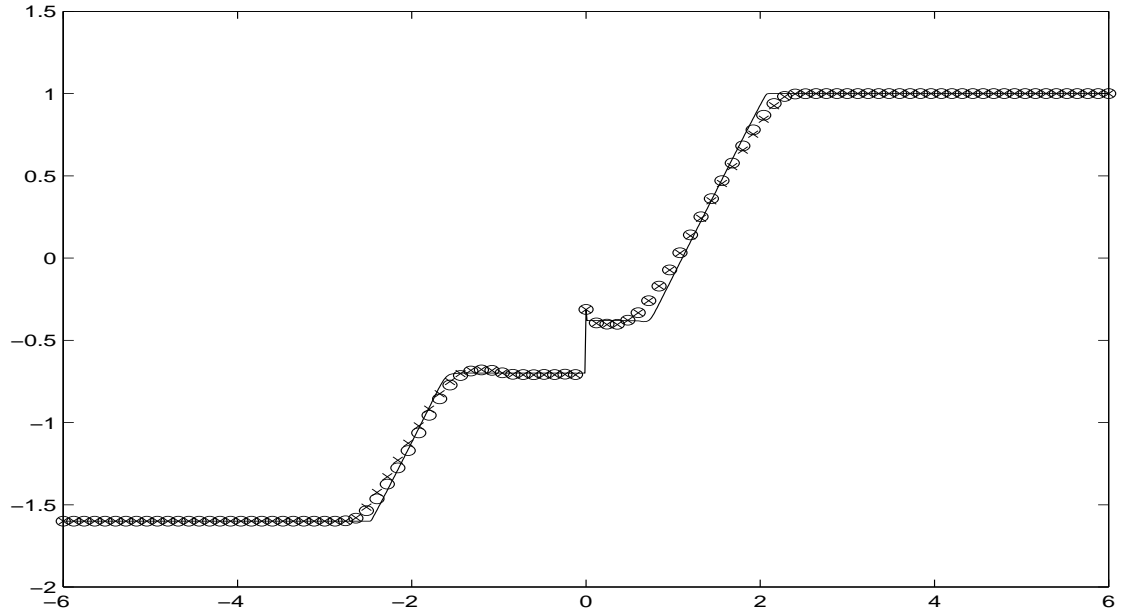
$$\rho(x, 0) = 4, \quad v(x, 0) = \frac{3}{\rho(x, 0)a(x)}. \quad (3.58)$$

The problem is solved numerically on domain $[-6, 6]$. The boundary conditions are given by $\rho v|_{x=-6} = 1.2$, $\rho|_{x=6} = 4$. We take $\frac{\Delta t}{\Delta x} = 1/2$. Figure 3.3 shows respectively the numerical steady state solutions of density, Mach number and energy. The results using 100 cells are similar to that using 400 cells. They also show that energy equals at both sides of cross-sectional discontinuity with a satisfactory accuracy.

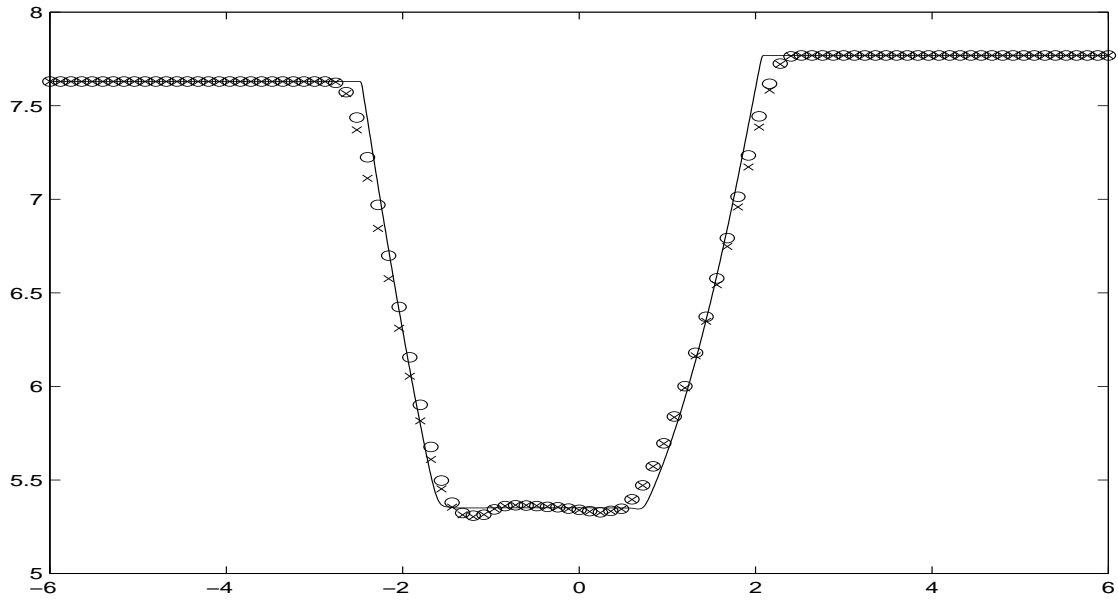
Remark: For Example 3.2 the Godunov solver encounters the "slow convergence" phenomenon more severely than the Roe solver. So we used the Roe solver instead. For this problem the Roe solver encounters the "slow convergence" phenomenon when L^∞ error between numerical solutions at two adjacent time step is about 10^{-3} . According to the study in [16], the "slow convergence" phenomenon is related to the stability of the discrete viscous profile of the used scheme and can be alleviated by using scheme having larger viscosity. For this problem, the HLLE solver and relaxation scheme are the likely candidates with an improved convergence speed. Since both these schemes provide just the interface values of the mass and momentum fluxes, from which one needs iterative schemes (such as Newton's method) at every grid point to obtain the interface values of the conserved variables, so they cannot be applied to the two interface type methods presented in this paper. An alternative method which can be combined with more general shock capturing methods, in addition to the Roe or Godunov method, is developed in [29].



(a): Density.



(b): velocity.



(c): energy.

Figure 3.1 Example 3.1, the mixed sub- and super-sonic case. Solutions at $t=0.8$. Solid line: the exact solution; "o": solution by the mass-energy method using 100 cells; "x": solution by the complete form method using 100 cells.

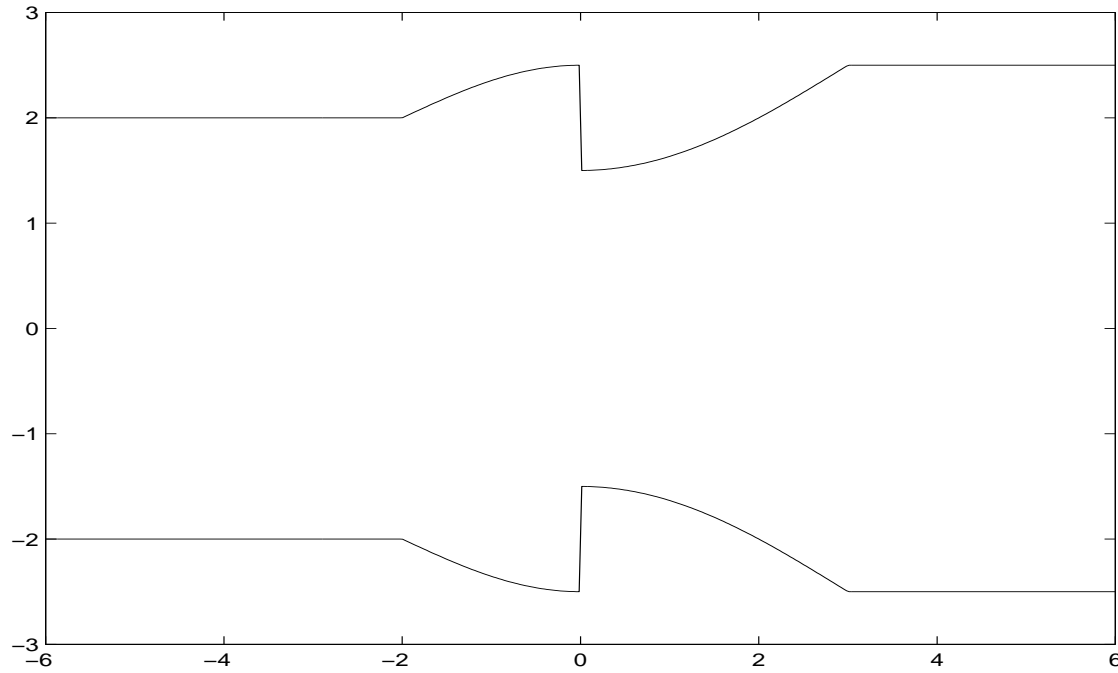
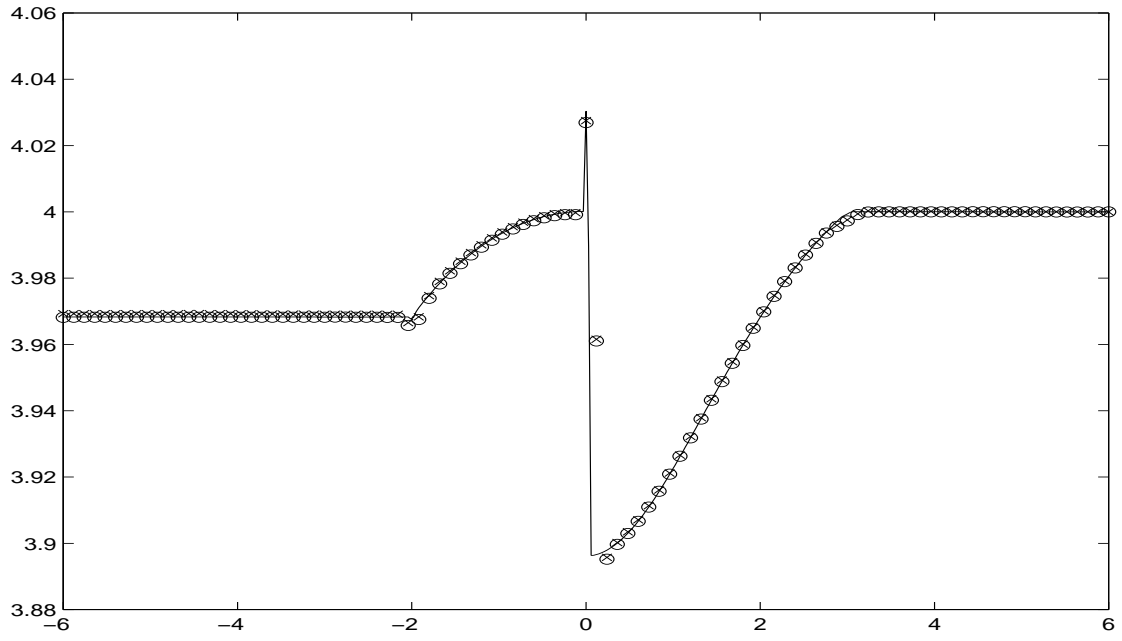
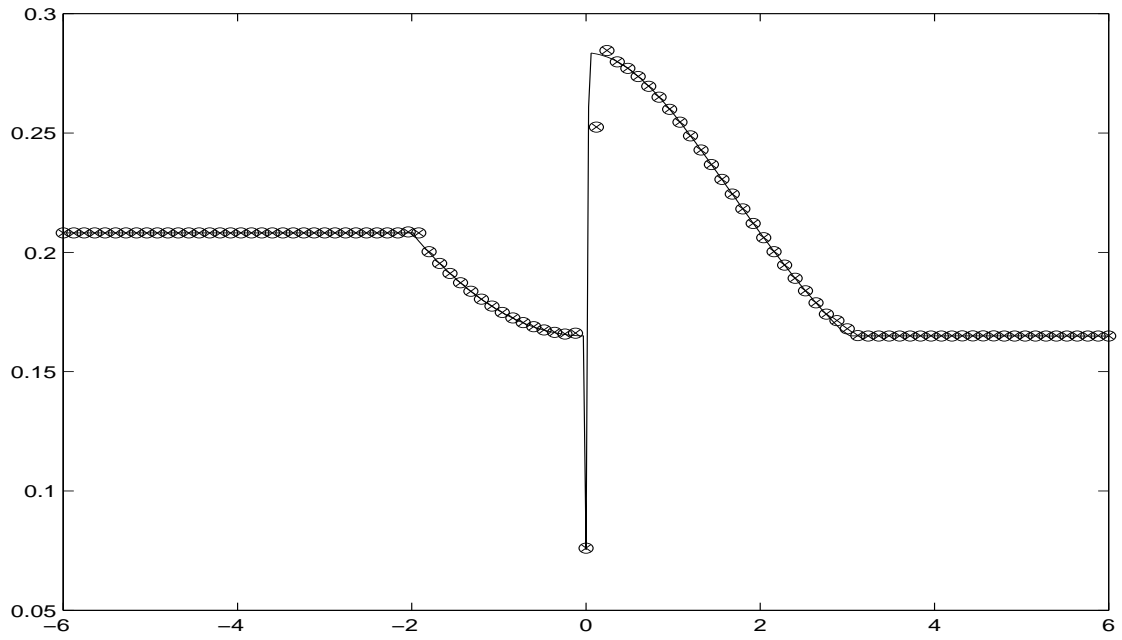


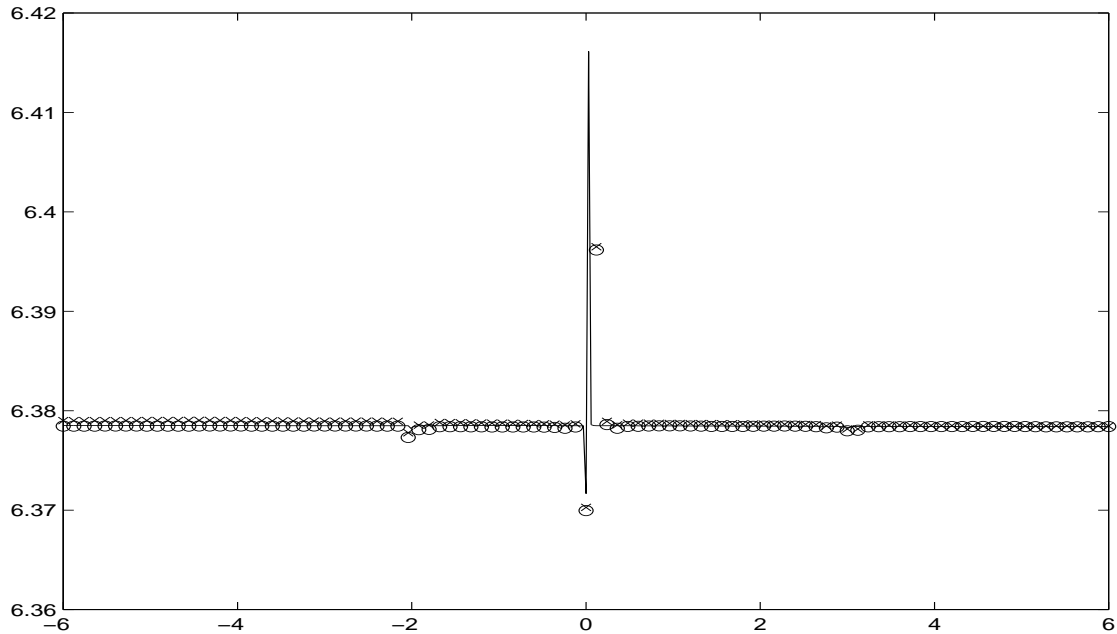
Figure 3.2 Example 3.2, the steady state case. The nozzle shape for the problem.



(a): Density.



(b): Mach number.



(c): energy.

Figure 3.3 Example 3.2, the steady state solutions. Solid line: solution of the complete form method using 400 cells; "o": solution of the complete form method using 100 cells; "x": solution of the mass-energy method using 100 cells.

4 Conclusions

Two simple well-balanced methods are proposed for hyperbolic system with geometrical source terms having concentrations. We use two physical problems, the shallow water equations with topography, and the quasi one-dimensional isothermal nozzle flows, to illustrate the basic methods. The advantage of the two methods is that they use the numerical fluxes already obtained from the corresponding homogeneous systems in the source terms. One only needs a black-box (approximate) Riemann solver for the homogeneous system. Compared to our previous method developed in [17], these new methods avoid the Newton iterations in the evaluation of the source term. Extensive numerical experiments demonstrate that both methods give good numerical approximations to the sub- and super-critical flows, and, with a transonic fix, to the the transonic flows over the concentration in both the steady and unsteady cases.

These ideas have the potential to be applicable to other related problems. Examples include the Euler flows with an exterior field (such as the Euler-Poisson system and the Euler-Maxwell system), and the classical Liouville or Vlasov equation with a discontinuous potential. These applications are currently under our study.

References

- [1] F. Alcrudo and F. Benkhaldoun, Exact solutions to the Riemann problem of the shallow water equations with a bottom step, *Computers Fluids* 30, 643-671 (2001).
- [2] E. Audusse, F. Bouchut, M.-O. Bristeau, R. Klein and B. Perthame, A fast and stable well-balanced scheme with hydrostatic reconstruction for shallow water flows, *SIAM J. Sci. Comp.*, to appear.
- [3] A. Bernudez and M.E. Vazquez, Upwind methods for hyperbolic conservation laws with source terms, *Computers Fluids* 23, 1049-1071 (1994).
- [4] R. Botchorishvili, B. Perthame and A. Vasseur, Equilibrium schemes for scalar conservation laws with stiff sources, *Math. Comp.* 72(241), 131-157 (2003).
- [5] A. Chinnayya and A.Y. Le Roux, A new general Riemann solver for the shallow-water equations with friction and topography, preprint 1999.
- [6] A.I. Delis, Improved application of the HLLC Riemann solver for the shallow water equations with source terms, *Commun. Numer. Meth. Engng.* 19, 59-83 (2003).
- [7] A.I. Delis and Th. Katsaounis, Relaxation schemes for the shallow water equations, *Int. J. Numer. Meth. Fluids* 41, 695-719 (2003).
- [8] T. Gallouët, J.-M. Hérard and N. Seguin, Some approximate Godunov schemes to compute shallow-water equations with topography, *Computers Fluids* 32, 479-513 (2003).
- [9] S.K. Godunov, Finite difference schemes for numerical computation of solutions of the equations of fluid dynamics, *Math. USSR Sbornik* 47, 271-306 (1959).
- [10] L. Gosse, A well-balanced flux-vector splitting scheme designed for hyperbolic systems of conservation laws with source terms, *Comp. Math. Appl.* 39, 135-159 (2000).
- [11] L. Gosse, A well-balanced scheme using non-conservative products designed for hyperbolic systems of conservation laws with source terms, *Math. Models Methods Appl. Sci.* 11(2), 339-365 (2001).
- [12] L. Gosse and A.-Y. Le Roux, A well-balanced scheme designed for inhomogeneous scalar conservation laws, *C.R. Acad. Sc., Paris. Sér I* 323, 543-546 (1996).

- [13] J.M. Greenberg and A.-Y. Le Roux, A well-balanced scheme for the numerical processing of source terms in hyperbolic equations, *SIAM J. Num. Anal.* 33, 1-16 (1996).
- [14] J.M. Greenberg, A.-Y. Le Roux, R. Baraille and A. Noussair, Analysis and approximation of conservation laws with source terms, *SIAM J. Num. Anal.* 34, 1980-2007 (1997).
- [15] S. Jin, A steady-state capturing method for hyperbolic system with geometrical source terms, *Math. Model. Num. Anal.* 35, 631-646 (2001).
- [16] S. Jin and J.-G. Liu, The effects of numerical viscosities I. slowly moving shocks, *J. Comp. Phys.* 126, 373-389 (1996).
- [17] S. Jin and X. Wen, An efficient method for computing hyperbolic systems with geometrical source terms having concentrations, *J. Comp. Math.* 22, 230-249, 2004.
- [18] A. Kurganov and D. Levy, Central-upwind schemes for the Saint-Venant system, *Math. Model. Numer. Anal.* 36(3), 397-425 (2002).
- [19] P.G. LeFloch and M.D. Thanh, The riemann problem for fluid flows in a nozzle with discontinuous cross-section, *Comm. Math. Sci.* 1, 763-797 (2003).
- [20] R.J. LeVeque, *Numerical Methods for Conservation Laws*, Birkhauser-Verlag, Basel, 1990.
- [21] R.J. LeVeque, Balancing source terms and flux gradients in high-resolution Godunov methods: the quasi-steady wave-propagation algorithm, *J. Comp. Phys.* 146, 346-365 (1998).
- [22] Ch. Makridakis and Th. Katsaounis, Relaxation models and finite element schemes for the shallow water equations, in *Hyperbolic Problems: Theory, Numerics, Applications*, Proceedings of the Ninth International Conference on Hyperbolic Problems held in CalTech, Pasadena, March 25-29, 2002 Hou, Thomas Y.; Tadmor, Eitan (Eds.)
- [23] B. Perthame and C. Simeoni, A kinetic scheme for the Saint-Venant system with a source term, *CALCOLO* 38(4), 201-231 (2001).
- [24] J.J. Quirk, *Int. J. Num. Methods Fluids* 18, 555 (1994).
- [25] P.L. Roe, Approximate Riemann solvers, parameter vectors, and difference schemes, *J. Comp. Phys.* 43, 357-372 (1981).
- [26] P.L. Roe, Upwinding differenced schemes for hyperbolic conservation laws with source terms, in *Nonlinear Hyperbolic Problems*, Proc. Adv. Res. Workshop, St. Étienne, 1986, Lect. Notes Math., Springer, Berline, 1270, 41-45 (1987).

- [27] M.E. Vazquez-Cendon, Improved treatment of source terms in upwind schemes for shallow water equations in channels with irregular geometry, *J. Comp. Phys.* 148, 497-526 (1999).
- [28] J.W. Wang and R.X. Liu, A comparative study of finite volume methods on unstructured meshes for simulation of 2D shallow water wave problems, *Mathematics and Computers in Simulation* 53,171-184 (2000).
- [29] X. Wen, in preparation.
- [30] K. Xu, A well-balanced gas-kinetic scheme for the shallow water equations with source terms, *J. Comp. Phys.* 178(2), 533-562 (2002).
- [31] J.G. Zhou, D.M. Gauson, D.M. Ingram and C.G. Mingham, Numerical solutions of the shallow water equations with discontinuous bed topography, *Int. J. Numer. Meth. Fluids* 38, 769-788 (2002).
- [32] J.G. Zhou, D.M. Gauson, C.G. Mingham and D.M. Ingram, The surface gradient method for the treatment of source terms in the shallow water equations, *J. Comp. Phys.* 168, 1-25 (2001).